Lawrence Berkeley National Laboratory
LBL Publications

Title

In Situ Characterization of Electrode Processes by Photothermal Deflection Spectroscopy

Permalink

https://escholarship.org/uc/item/9h96z9ng

Authors

Rudnicki, J D
McLarnon, F R
Cairns, E J

Publication Date

1989-04-01
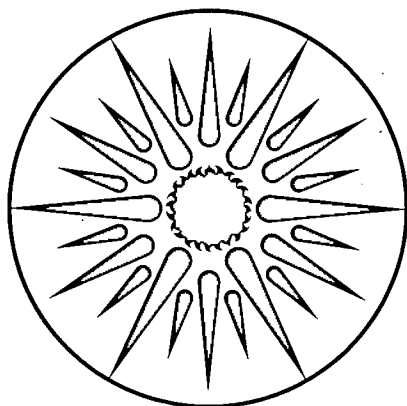
Lawrence Berkeley Laboratory
UNIVERSITY OF CALIFORNIA

APPLIED SCIENCE
DIVISION

In Situ Characterization of Electrode Processes by Photothermal Deflection Spectroscopy

J.D. Rudnicki, F.R. McLarnon, and E.J. Cairns

April 1989

APPLIED SCIENCE
DIVISION

DISCLAIMER

IN SITU CHARACTERIZATION OF ELECTRODE PROCESSES BY PHOTOTHERMAL DEFLECTION SPECTROSCOPY

by

James D. Rudnicki, Frank R. McLarnon, and Elton J. Cairns

Applied Science Division
Lawrence Berkeley Laboratory
1 Cyclotron Road
Berkeley, California 94720

April 1989

In Situ Characterization of Electrode Processes by Photothermal Deflection Spectroscopy

James D. Rudnicki, Frank R. McLarnon, and Elton J. Cairns

*Applied Science Division, Lawrence Berkeley Laboratory,
and Department of Chemical Engineering,
University of California, Berkeley, California 94720*

I. Introduction

Photothermal deflection spectroscopy (PDS) is a versatile *in situ* surface-sensitive technique applicable to the study of electrochemical interfaces. The technique was originally developed by Boccara, Fournier, and Badoz (1,2). PDS is also called Photothermal Beam Deflection Spectroscopy (PBDS) or mirage effect spectroscopy. PDS can measure the absorption spectrum of electrode surface species with submonolayer sensitivity, the absorption spectrum of electrolyte species, and the concentration gradients near the electrode surface.

Photothermal techniques are quite versatile. Besides the most common use: measuring either homogeneous-phase or interfacial absorption spectra, photothermal techniques have been applied to chromatography, fluid dynamics, and material characterization (3-7).[1] The principles of all the photothermal techniques are similar; this chapter will discuss the aspects of PDS applicable to electrode surfaces.

A simplified diagram of a PDS system is shown in Figure 1. The basis of PDS is the detection of refractive-index gradients in the electrolyte adjacent to

[1] Reference 5 contains a comprehensive discussion of the many applications of photothermal techniques.

source

monochromator

chopper

probe beam   L   cell   PD
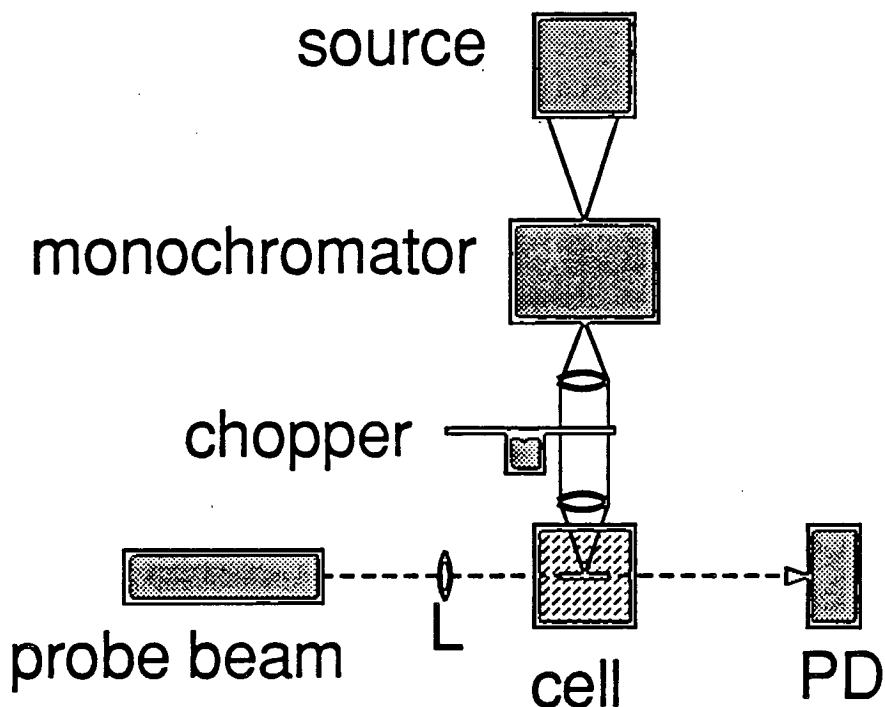
Figure 1. A basic PDS system. The source provides broadband light which is dispersed by the monochromator. The narrowband excitation light leaving the monochromator is modulated by a mechanical chopper and focused onto the electrode. The probe beam passes parallel to the electrode surface. Deflections of the probe beam are detected with the position detector (PD).

the electrode. These gradients are measured by the deflections of a probe beam passing through the gradients. Section II of this chapter describes the processes which cause probe-beam deflections and their measurement. Section III discusses the major components of a PDS system. Section IV presents the results of the study of several electrochemical systems.

PDS has several advantages compared to existing spectro-electrochemical techniques. First, PDS uses a relatively low-intensity excitation light of approximately 10^{-2} $W \cdot cm^{-2}$ to probe the interface. The risk of inducing changes in the surface chemistry is much

smaller than with the high-intensity laser techniques using up to 10^5 W·cm^{-2}, e.g. Raman and second harmonic generation (SHG). Second, PDS is applicable to any electrochemical interface. The electrode surface is only required to be approximately planar; polished, smooth, porous, and rough surfaces can be studied. Last, the advantages of in situ techniques cannot be under-stated (8). Only the in situ techniques can monitor transient processes. The in situ techniques do not require the removal of the electrode from the electrochemical environment, which can alter the identity or structure of the surface species. Armstrong and Muller (9) have studied copper electrodeposits with in situ scanning tunneling microscopy (STM) and have shown that the microtopography changes after 1 minute at open circuit. This demonstrates the problem of removal of electrodes from the electrochemical environment; a problem not encountered by in situ techniques.

II. Theory

The basis of PDS, with reference to an electrochemical system, is the generation and measurement of gradients in the refractive index of the electrolyte adjacent to an electrode. The transverse geometry shown in Figure 1 will be the basis of discussion. With this geometry, the excitation light is applied normal to the

electrode surface, and a probe beam (typically a laser)
is passed parallel to the electrode surface. The
presence of a gradient in the refractive index will cause
an angular deflection of the probe beam. The deflection
of the probe beam by a refractive index gradient is
discussed in Section A, below. The refractive index is a
function of temperature and composition of the
electrolyte. Three processes can generate refractive
index gradients: 1)absorption of light at the interface,
2)electrochemical reactions at the interface, and
3)absorption of light in the electrolyte. These
processes are discussed in Sections B, C, and D,
respectively. Section E discusses thermal effects which
can complicate the analysis of experimental data.

A. Deflection of the Probe Beam

The refractive index gradient is measured by passing
a probe laser beam parallel to the electrode surface.
The deflection of a ray is described by (10)

$$\frac{d}{ds}\left[n_0\frac{dr_0}{ds}\right] = \nabla n(r,t) \, , \tag{1}$$

where S is the ray path, n_0 is the bulk refractive index,
r_0 is the perpendicular displacement of the ray from its
original direction, and $\nabla_\perp n(r,t)$ is the gradient of the
refractive index perpendicular to the ray path. For a
typical situation with the gradient only in the x

direction (see Figure 2), the above equation is simplified to (many references discuss this, e.g. 11,12):

$$\frac{d}{ds}\left[n_0\frac{dx}{ds}\right] = \frac{\partial n(x,t)}{\partial x} \ . \tag{2}$$

The deflections of the probe beam are typically small. Angular deflections of 1 μrad are common and the detection limit is on the order of 1 nrad (11,13). Because of the small angular deflections, the distance between the probe beam and electrode surface is approximately constant and $\partial n(x,t)/\partial x$ will not change over the path of the probe beam. Also because of the small deflections, dx/ds is approximately the angular deflection of the beam, θ. Integration of Equation [2] results in the well-known formula:
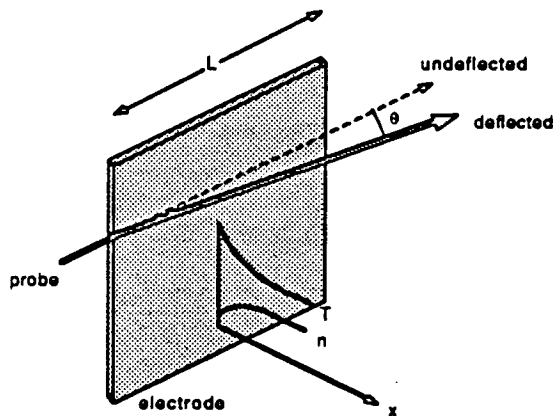
Figure 2. Diagram of the electrode showing a refractive index profile ,n, caused by the temperature profile, T. The refractive index gradient causes an angular deflection of the probe beam, θ.

$$\theta(x,t) = \frac{L}{n_0}\cdot\frac{\partial n(x,t)}{\partial x} \ , \tag{3}$$

where θ is the angular deflection measured from the leading edge of the electrode, and L is the length of the

electrode. This is a statement of the familiar Schlieren effect.

In the above derivation of Equation [3], much is based on the assumption that the probe beam deflections are small. For conventional PDS this assumption is valid, but for some electrochemical systems, concentration gradients can cause large deflections which would make Equation [3] invalid. For such systems, a more-general form of Equation [3] can be derived from Equation [2]. This requires an expression for $n(x,t)$, which for any given reaction can be derived from the governing diffusion equations. Often the reaction mechanism is unknown however, and Equation [3] must be used as a first approximation.

The other major assumption in the above derivation is that the probe beam has an infinitesimal diameter. Typically the refractive index profile in the electrolyte is curved, i.e. as is shown in Figure 2, dn/dx varies with x. Because the probe beam has a finite diameter, different regions of the beam are affected by gradients of different magnitude. As a result, the beam distorts as it deflects. Mandelis and Royce derived an analytical solution for the deflection and distortion of a circular beam in a concentration gradient (14). Their results show that the beam develops an elliptical shape as it

deflects[2]. The dimensions of the ellipse contain
information about the curvature of the refractive-index
gradient, which is related to the diffusion coefficient
of the chemical species. The results also show that the
elliptical distortion is not large and should be
negligible in most situations.

To relate Equation [3] to more meaningful
quantities, the refractive index of the electrolyte can
be approximated by a Taylor series expansion with only
the first-order terms included:

$$n \simeq n_0 + (T-T_0) \left. \frac{\partial n}{\partial T} \right|_{T=T_0} + (C-C_0) \left. \frac{\partial n}{\partial C} \right|_{C=C_0} , \qquad [4]$$

where T is temperature, C is concentration (a binary
electrolyte is assumed), and the partial derivatives are
evaluated at the point of the expansion. Taking the
derivative of this expansion with respect to x results in

$$\frac{dn}{dx} = \frac{dT}{dx} \cdot \frac{\partial n}{\partial T} + \frac{dC}{dx} \cdot \frac{\partial n}{\partial C} . \qquad [5]$$

This equation apparently shows that a single measurement
of the probe beam deflection, and therefore dn/dx, cannot
determine both dT/dx and dC/dx (the physical parameters,

---

[2] This effect is the basis of Thermal Lensing Spectroscopy,
a related technique which measures the curvature of the
refractive index as opposed to PDS which measures the
gradient of the refractive index.

$\partial n/\partial T$ and $\partial n/\partial C$ are known). The following section will
show that modulation of the excitation light allows dT/dx
to be separated from dC/dx.

B. Electrode Surface Optical Absorption

This section begins with a qualitative description
of the photothermal deflection effect and concludes with
a discussion of the results of mathematical models of
PDS.

The absorption of light at the electrochemical
interface is the primary process studied with PDS. Light
is directed through the electrolyte onto the electrode
surface. Light which is absorbed at the interface is
converted to heat within a negligible time by non-
radiative relaxation processes[3] (7). The temperature of
the interface increases, and conduction of heat away from
the interface (into both the electrolyte and electrode
phases), causes temperature gradients in both phases.
Many electrolytes exhibit a decrease in refractive index
as temperature increases. For such an electrolyte, the
heating of the interface causes the refractive index of
the electrolyte to be lowered adjacent to the electrode.
The probe beam will be deflected away from the electrode,

---

[3] Some electrode surfaces may exhibit behaviors
contradictory to this statement, e.g. florescence,
phosporescence, and photocurrents. Such systems must be
treated in a more-complex manner; see Reference 47.

as indicated in Figure 2. This process, in which light is absorbed, converted to heat, and causes a deflection of the probe beam is the *photothermal deflection* effect.

Modulation of the excitation light and lock-in detection of the probe beam deflection is used by PDS. During the time the excitation light illuminates the electrode, the interface heats and the thermal gradient propagates into the electrolyte. The gradient relaxes during the time the excitation light is off. The probe beam thereby exhibits periodic deflections. These deflections are called the AC component. A lock-in amplifier is used to measure the magnitude of only those deflections which are at the same frequency as the modulation frequency.

The probe beam passes through the electrolyte at a small but finite distance from the electrode. A delay therefore exists between the time when the excitation light is converted to heat at the interface and the time when the heat has been conducted to the position of the probe beam. The delay is expressed as a phase (expressed as an angle between 0° and 360°), and is measured by the lock-in amplifier. The signal phase is a function of modulation frequency, and is discussed below.

To distinguish the deflection of the probe beam caused by absorption of light at the interface from other

components of the deflection (to be discussed in the following sections) and because the phase is variable, it is referred to as the 'AC deflection at x°'. By varying the wavelength of the excitation light, and measuring the AC deflection at x°, an absorption spectrum of the interface is obtained.

To obtain a quantitative description of the AC deflection at x°, the thermal conduction equations must be solved. Such a solution will describe the relationship between the AC signal at x° and the absorption coefficient of the electrode surface, the modulation frequency, the excitation light intensity, and the physical dimensions of the system. Since the geometry of the system is intrinsic to the solution, there are no general equations which describe the temperature profiles.

Many system geometries have been studied experimentally and theoretically, e.g. thermally thin or thick samples, multiple layer samples, samples mounted on a thermally insulating or conductive substrate, and samples mounted on an optically opaque or transparent substrates. Analytic solutions of several system geometries reported are in the literature (11,12,15-20). Because PDS was originally developed as a spectroscopic technique applicable to solid, liquid, and gas samples, most solutions have been developed in a less-restricted

context where the sample is not opaque[4]. These solutions are, however, applicable to a metallic electrode if we assume a large extinction coefficient.

A geometry examined by Murphy and Aamodt displays behavior characteristic of all systems and will be used to demonstrate the relationship between the AC signal and various parameters (21). The sample was a 200 nm thick Pt film sputtered onto a glass substrate. The heating of the Pt surface caused by the excitation light was simulated by ohmic heating of the film by its own resistance. The ohmic heating causes a uniform heating above the Pt surface, which is sensed by the probe beam with a transverse arrangement similar to that shown in Figure 1. The theoretical derivation predicts

$$\ln S \propto \frac{-x_0}{\mu} \ , \ \ \phi \propto \frac{-x_0}{\mu} \ , \ \text{and} \ \mu \equiv \sqrt{\frac{\alpha}{\pi f}} \ , \quad\quad [6]$$

where S is the signal amplitude (proportional to the probe beam deflection), ϕ is the signal phase, μ is the thermal diffusion length, x_0 is the offset of the probe beam from the Pt surface, α is the thermal diffusivity of the deflecting medium and f is the modulation frequency.

---

[4] Some temperature profiles also originated from the field of photoacoustic spectroscopy (PAS). This technique illuminates a solid sample with modulated excitation light. Therefore, solutions of the thermal equations are applicable to PDS with little or no modification.

These relations were tested experimentally. Figure 3 shows the signal amplitude and phase as a function of the probe beam offset. The four curves in each plot are for increasing levels of heating, which simulates increasing optical absorption at the Pt surface (the Pt film is thermally thin and therefore heating of the surface is equivalent to bulk heating). The plots show the linear behavior predicted by Equation [6]. The exponential dependence of S on x_O is characterized by the thermal diffusion length; the signal amplitude decreases by 63% for each thermal diffusion length the probe beam moves away from the surface. The experiments in Figure 3 were performed in air where μ = 446 μm. In an aqueous electrolyte at f=40 Hz, μ is about 34 μm. Therefore, in electrochemical systems the probe beam must be positioned close to the electrode surface to achieve maximum signal amplitude.

Equation [6] also shows that the logarithm of the signal amplitude decreases with $\sqrt{f}$ and that the signal phase varies linearly with $\sqrt{f}$. This relationship limits the usable modulation frequency to low values. In liquids, modulation frequencies are commonly about 10 to 40 Hz, although some experiments have used up to 250 Hz. Equation [6] also indicates a method of determining the offset of the probe beam. A plot of ln S vs. $\sqrt{f}$ or ϕ vs.
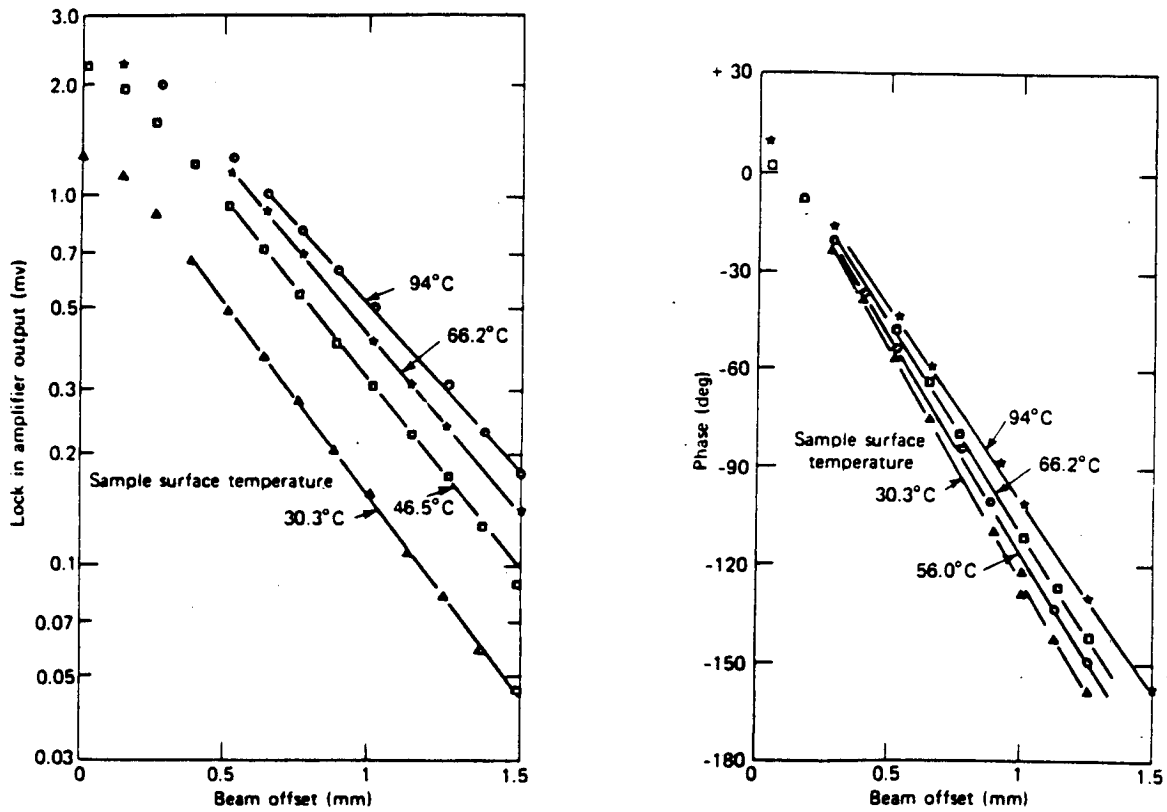
Figure 3. Experimental data for logarithm S *vs.* x_0 and ϕ *vs.* x_0 for four heating levels. The curves are marked with the average surface temperature, representative of different levels of optical absorption at the surface. The modulation frequency was 40 Hz and the deflecting medium was nitrogen. [reprinted by courtesy from reference 15]

$\sqrt{f}$ will have a slope of $-x_0 \sqrt{(1/2\alpha)}$, from which x_0 can be determined.

Murphy and Aamodt (21) predicted theoretically and confirmed experimentally that the PDS signal amplitude increased linearly with increasing power of the excitation light (an important requirement). An experimental and theoretical evaluation of the dependence of signal amplitude on the angle between the probe beam and electrode surface showed that the signal amplitude was maximized when the probe beam was aligned parallel to the electrode surface. Qualitatively, the relationship

of signal amplitude and

phase to experimental

conditions described by

Murphy and Aamodt is

applicable to all PDS

systems

    Lasalle, *et. al.*

determined the effect of

the finite diameter of

the probe beam on the PDS

signal (22). The

geometry was a solid

sample immersed in a

liquid where the

excitation light was a

focused laser beam. When

the probe beam radius is

Figure 4. Theoretical plots of (A) logarithm of the signal amplitude *vs.* $\sqrt{f}$ and (B) signal phase *vs.* $\sqrt{f}$. The deflecting medium has $\alpha=3\times10^{-8}$ m^2s^{-1}, the probe beam radius is 64 μm, and the excitation beam radius is 130 μm. The ten curves represent increasing probe beam offsets (in μm): 1) 100, 2) 120, 3) 130, 4) 140, 5) 150, 6) 160, 7) 170, 8) 180, 9) 200, and 10) 220. [reprinted by courtesy from reference 22]

less than the thermal diffusion length, μ, the probe beam

behaves as a single ray. But, as the probe beam radius

increases relative to μ, the behavior of the probe beam

becomes complex. Figure 4 shows the predicted behavior

of signal magnitude and phase as a function of modulation

frequency. At low modulation frequencies, the signal

magnitude behaves as predicted from Equation [6]. At 80

Hz the signal undergoes a change, appropriately called

"catastrophic" by Lasalle, *et. al.*. In the catastrophic

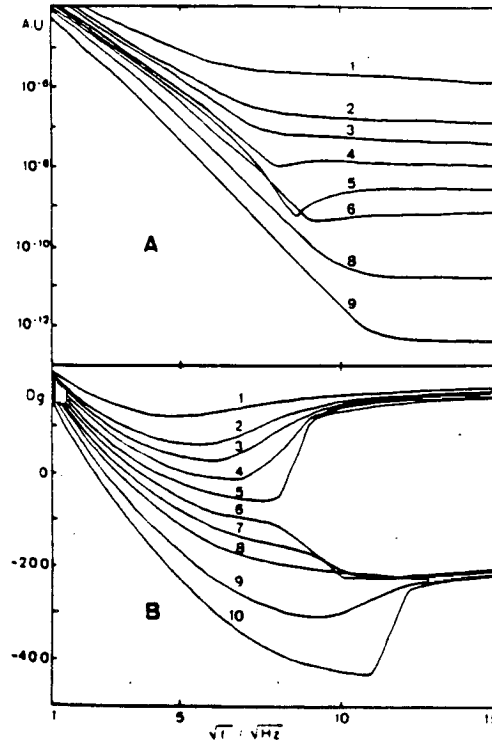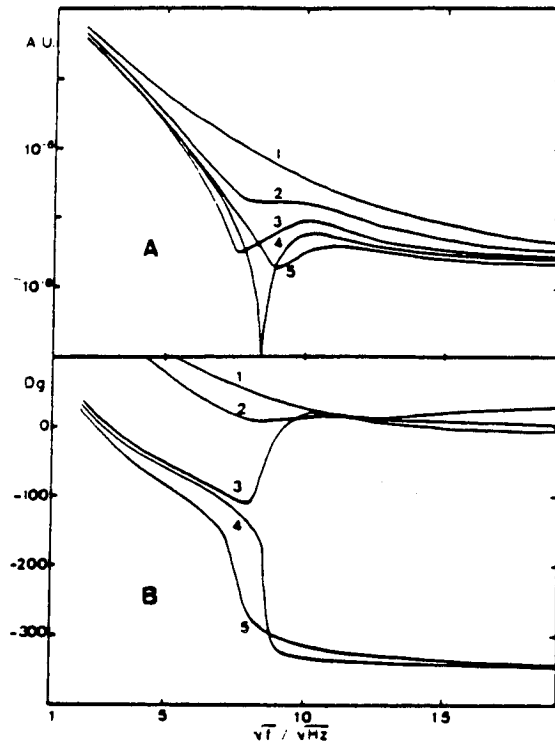region the signal magnitude displays a minimum or change

Figure 5. Experimental plots of (A) logarithm of the signal amplitude vs. $\sqrt{f}$ and (B) signal phase vs. $\sqrt{f}$. The deflecting medium is liquid paraffin, the probe beam radius is 64 μm, and the excitation beam radius is 130 μm. The five curves represent increasing probe beam offsets (in μm): 1) 110, 2) 130, 3) 148, 4) 153, and 5) 158. [reprinted by courtesy from reference 22]

in slope. The signal phase changes sharply in the catastrophic region. Experimental confirmation of this behavior is shown in Figure 5. The experiment displays the minima in the signal magnitude and the abrupt phase change predicted by the theory, although the quantitative agreement is not exact. The physical origin of the disturbances in the catastrophic frequency range is not evident from the theory. It may be that the small diameter of the excitation light is the cause of this behavior. The effects described above are avoided if a low modulation frequency is used; this is also desirable in order to achieve maximum signal amplitude as described above.

C. Non-selective Measurement of Concentration Gradients

Electrochemical reactions will cause concentration gradients and corresponding refractive index gradients in the electrolyte. The systems studied involve

electrochemical reactions which generate gradients which

vary slowly, compared to the AC deflection at x°. The

deflection caused by concentration gradients is referred

to as the 'DC deflection'. The AC deflection at x° is

superimposed upon the DC deflection.

For a single-solute electrolyte, measurement of the

DC deflection provides direct information about the

concentration gradient. For a two-solute electrolyte,

Equation [5] is extended to

$$\frac{dn}{dx} = \frac{dT}{dx} \cdot \frac{\partial n}{\partial T} + \frac{dC_1}{dx} \cdot \frac{\partial n}{\partial C_1} + \frac{dC_2}{dx} \cdot \frac{\partial n}{\partial C_2} . \qquad [7]$$

From a single measurement of dn/dx, the concentration

gradients of species 1 and 2 are indeterminate. Because

of the inability to discern individual concentration

gradients for electrolytes with two or more solutes, the

DC deflection measurement is referred to as the non-

selective measurement of concentration gradients (a

selective measurement method is described in the next

section).

Assumptions can be made to overcome the

non-selectivity of the DC deflection. A background or

"blank" experiment can be performed with only one

component present in the electrolyte. If the chemistry

is assumed unchanged by the addition of the second

component, then the background can be subtracted from the

results of the experiment with both components. In other situations, one of the terms of Equation [7] may dominate the sum; either one concentration gradient can be much larger than the other, *i.e.* $dC_1/dx \gg dC_2/dx$, or one species can have a larger effect on the refractive index than the other, *i.e.* $\partial n/\partial C_1 \gg \partial n/\partial C_2$.

The DC deflection can be used to determine diffusion coefficients of electrolyte species when the reaction mechanism is known. The response of the reaction

$$O + ne^- \leftrightarrow R,$$
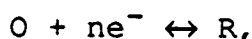
to a potential step experiment has been treated by Pawliszyn in Reference 23. Initially, the reactant (O) was assumed to be at uniform concentration, C^O, and the product was assumed to have zero concentration. Assuming diffusion control and fast kinetics, the concentration profiles for the reactant and product are

$$C_O(x,t) = C^O \, \text{erf}\left[\frac{x}{\sqrt{4D_O t}}\right] \text{, and} \tag{8a}$$

$$C_R(x,t) = C^O \, \text{erfc}\left[\frac{x}{\sqrt{4D_R t}}\right]. \tag{8b}$$

Here t is the time measured from the beginning of the potential step and x is the distance from the electrode. The concentration gradients will be

$$\frac{\partial C_O}{\partial x} = \frac{C^O}{\sqrt{\pi D_O t}} \, \exp\left[\frac{-x^2}{4D_O t}\right] \text{, and} \tag{9a}$$

$$\frac{\partial C_R}{\partial x} = \frac{-C^o}{\sqrt{\pi D_R t}} \exp\left[\frac{-x^2}{4D_R t}\right].$$ [9b]

The diffusion coefficients for reactant and product will be assumed equal. Substitution of equations [9a] and [9b] into equation [7] results in the following expression for the refractive index gradient

$$\frac{dn}{dx} = \frac{C^o}{\sqrt{\pi D_O t}}\left[\frac{dn}{dC_O} - \frac{dn}{dC_R}\right]\exp\left[\frac{-x^2}{4D_O t}\right].$$ [10]

Equation [10] predicts that from a single potential step experiment, the diffusion coefficient can be determined. This determination requires that the distance of the probe beam from the electrode surface be known. Experimentally, accurate determination of the probe beam-electrode distance is difficult. To overcome this problem, the time of the maximum deflection can be measured for several positions of the probe beam (the relative position of the probe beam can be accurately controlled with a micrometer translation stage), and a plot of t_{max} versus x_o^2 will be a straight line with slope 1/2D.

Mandelis and Royce (14) derived the response of the probe beam deflection to a potential step and, in contrast to Pawliszyn, concluded that the maximum of the beam deflection occurs at $x_o^2/4D$. Experimental results support this conclusion. Royce, Voss and Bocarsley

applied the potential step technique to study the
ferri/ferrocyanide redox couple (24). Their results
showed that a plot of t_{max} versus x_o^2 was a straight
line. Based on the slope of the line being 1/4D, they
determined the diffusion coefficient of
ferri/ferrocyanide to be 9.4 x 10^{-6} cm^2 s^{-1}. This value
is 5-25% higher than literature values for the diffusion
coefficients of $Fe(CN)_6^{-3}$ and $Fe(CN)_6^{-4}$, e.g. Reference
25 reports 8.96 x 10^{-6} cm^2 s^{-1} and 7.39 x 10^{-6} cm^2 s^{-1}
and Reference 26 reports 8.9 x 10^{-6} cm^2 s^{-1} and 8.0 x 10^{-6} cm^2 s^{-1}, both for $Fe(CN)_6^{-3}$ and $Fe(CN)_6^{-4}$ respectively.

To explain some of the differences in the
literature, we have derived a more-general equation for
the response of the probe beam deflection to a potential
step. For a reaction:

$$A \leftrightarrow B + ne^-,$$
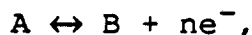
governed by fast reversible kinetics, the solution of the
diffusion equation for concentration yields:[5]

$$C_A(x,t) = C_A^o + \frac{\theta C_B^o - C_A^o}{1 + \theta\xi} \, \text{erfc}\left[\frac{x}{\sqrt{4D_A t}}\right], \text{ and} \qquad [11a]$$

$$C_B(x,t) = C_B^o - \frac{\xi(\theta C_B^o - C_A^o)}{1 + \theta\xi} \, \text{erfc}\left[\frac{x}{\sqrt{4D_B t}}\right]. \qquad [11b]$$

---

[5] Unpublished work. For a similar derivation, see reference
29.

where $C_A{}^O$ and $C_B{}^O$ are the bulk concentrations, $\theta \equiv \exp[nF/RT(E-E^O]$ and $\xi \equiv \sqrt{D_A/D_B}$. Taking the derivatives with respect to x and substituting into [7] yields:

$$\frac{\partial n}{\partial x} = \frac{-(\theta C_B^o - C_A^o)}{(1+\theta\xi)\sqrt{\pi D_A t}}\psi_A \exp\left[\frac{-x^2}{4D_A t}\right] + \frac{\xi(\theta C_B^o - C_A^o)}{(1+\theta\xi)\sqrt{\pi D_B t}}\psi_B \exp\left[\frac{-x^2}{4D_B t}\right], \qquad [12]$$

where $\psi_i \equiv dn/dC_i$. For a mass transfer limited step, $\theta = 0$ and Equation [12] is simplified to:

$$\frac{\partial n}{\partial x} = \frac{C_A^o}{\sqrt{\pi D_A t}}\psi_A \exp\left[\frac{-x^2}{4D_A t}\right] - \frac{\xi C_A^o}{\sqrt{\pi D_B t}}\psi_B \exp\left[\frac{-x^2}{4D_B t}\right]. \qquad [13]$$

This equation reveals quite varied behavior of the probe beam deflection, dependent on the values of the physical parameters.

Figure 6 is a plot of nine characteristic deflections of the probe beam, obtained from Equation [13]. This figure shows that the maxima of the probe beam deflections are not located at any unique time that would allow a simple determination of the species diffusion coefficients (the solid curves do correspond to the maximum reported by Pawliszyn at $x_o{}^2/2D$ in Reference 23). The figure also shows that the maxima are broad and therefore difficult to precisely determine from experimental data. A non-linear regression fitting Equation [13] to the experimental data may be able to determine the diffusion coefficients.

The physical properties from which Figure 6 was
calculated correspond to those of the ferri/ferrocyanide
redox couple. Specifically, curve 7 corresponds to a
cathodic potential step and curve 3 corresponds to an
anodic potential step. A slight reverse deflection is
seen for these curves between 0.25 and 0.75 s. This
effect is due to the difference in diffusion
coefficients. For curve 7, the reactant concentration
gradient increases more quickly than that of the product.
At short times therefore, the deflection is dominated by
the positive $\partial C_A/\partial x$. At long times, the negative $\partial C_B/\partial x$
dominates because $\psi_B > \psi_A$. The opposite explanation holds

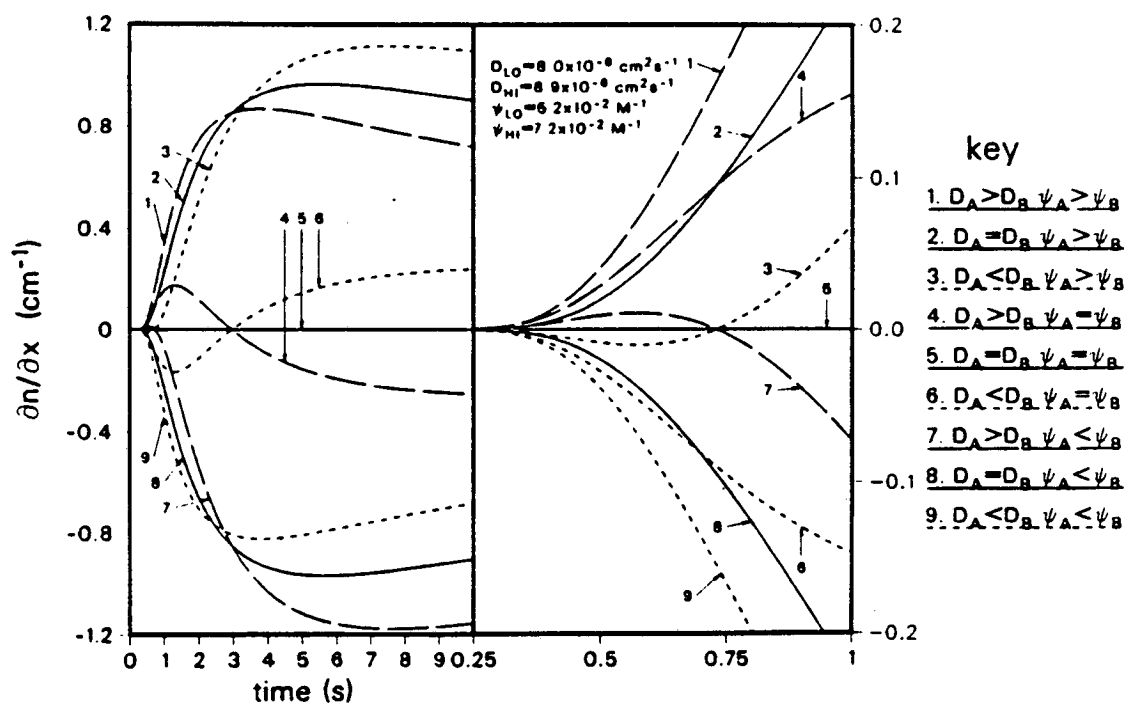Figure 6. Theoretical probe beam responses to a potential step experiment. The left figure
shows the behavior during the first 10 s, and the right figure is a magnification of the response
from 0.25 s to 1.0 s. The values of D_i and ψ_i were chosen from the values indicated in the
figure; when the parameters were equal, the higher value was used. $C_A{}^0$ was unity and x
was 100 μm.

for curve 3. This effect was experimentally observed in
Reference 24 and duplicated in our PDS system.

Decker, *et. al.*, (27) reported a sinusoidal current
technique to determine diffusion coefficients. This
technique avoids the problems of potential step
experiments and allows the use of lock-in detection,
resulting in increased signal-to-noise ratios. For a
reversible reaction modulated by a current, $I = I_0 \sin \omega t$,
the solution of the diffusion equation indicates that a
plot of the logarithm of the signal magnitude versus the
electrode-beam separation and signal phase versus the
electrode-beam separation are both straight lines with
slope $-\sqrt{(\omega/2D)}$. The reversible reaction

$$Cu^{2+} + 2e^- \leftrightarrow Cu$$
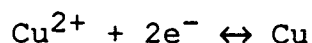
in 0.01 $\underline{M}$ $CuSO_4$ + 0.5 $\underline{M}$ H_2SO_4 at a Pt electrode was
studied. The magnitude and phase of the deflection of
the probe beam were measured with a lock-in amplifier.
The diffusion coefficient of Cu^{2+} was determined to be
1.1×10^{-5} cm^2 s^{-1}.

Pawliszyn, *et. al.* report a potential modulation
technique based on double-potential steps and triangular
potential sweep programs (28). The probe-beam
deflections were monitored with a lock-in amplifier. The
amplitude of the probe beam deflections are proportional
to the bulk concentration of electroactive species (see
Equation [13]). By measuring the amplitude of the probe-

beam deflections, they were able to measure the
concentration of oxygen dissolved in the electrolyte.
During their experiments, equilibration with the purge
gas caused the oxygen concentration to continuously
decrease. The PDS technique was determined to be at
least one order of magnitude more sensitive than
conventional cyclic voltammetry, *i.e.* current monitoring
techniques (29).

In the above methods, the reaction mechanism was
known. When the reaction is unknown, the DC deflection
can be used in conjunction with diffusion models as an
aid to the determination of mechanisms. Any proposed
reaction mechanism should be able to predict the observed
concentration gradients. If a theoretical model
disagrees with observation, the proposed mechanism can be
rejected. Agreement between the model and observation
lends support to a proposed mechanism, but cannot be
considered proof since many mechanisms can produce
similar effects. The systems described in Section IV
contain examples of the information about reaction
mechanism contained in the DC deflection behavior.

D. Selective Measurement of Concentration Gradients

As mentioned in the introduction, PDS can measure
homogeneous-phase absorption spectra. This ability can
be used to determine the concentration gradients of

individual components in a multi-component electrolyte or determine the absorption spectrum of the electrolyte.

Absorption of uniform-intensity excitation light in a region of the electrolyte where a concentration gradient exists will cause a temperature gradient in proportion to the concentration gradient of the absorbing species (21,23)·

$$\frac{dT}{dx} = \frac{I\varepsilon}{C_p\rho}\cdot\frac{dC}{dx} , \qquad [14]$$

where I is the intensity of the excitation light, ε is the absorptivity, C_p is the heat capacity of the electrolyte, and ρ is the density.[6] Since this gradient is caused by the modulated excitation light, the probe beam deflection it causes is periodic. No significant delay exists between when the electrolyte is illumina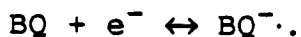ted and when the refractive index gradient is formed. Therefore, the deflections of the probe beam will have a 0° phase. This third component of the deflection is superimposed upon the other two and is referred to as the

---

[6] If the excitation light has a non-uniform intensity profile and the concentration is uniform, a temperature gradient is generated according to $dT/dx \approx (C\varepsilon/C_p\rho)\, dI/dx$ (the exact theory is more complex, see References 12 and 11). This is the basis of homogeneous phase PDS. Focusing of the excitation light onto the electrode surface results in an increasing intensity as the excitation light propagates towards the electrode, and can cause a signal.

'AC deflection at 0°'.
The method of separating
the two AC deflections is
based on their phase
difference and is
discussed below. By
varying the wavelength of
the excitation light, and
monitoring the AC
deflection at 0°, the
absorption spectrum of
the species causing the
concentration gradient in
the electrolyte can be
obtained.

Figure 7. Cyclic voltammogram and probe beam deflection for 6.3mM BQ in Me_2SO at 5 mV/s. The potential refers to a Ag wire psuedoreference electrode. The excitation wavelength was 470 nm. The probe beam deflection is due to optical absorption in the electrolyte by the $BQ^-\cdot$ reduction product. [reprinted by courtesy from reference 21]

Pawliszyn, et. al.,
studied the reduction of
p-benzoquinone (BQ) in dimethyl sulfoxide electrolyte at
a platinum electrode (21). The reversible reaction is

$$BQ + e^- \leftrightarrow BQ^-\cdot.$$

The product, $BQ^-\cdot$, has an absorption band at ~460 nm, and
the reactant is non-absorbing in the visible. Chopped
monochromatic excitation light illuminated the electrode
and the AC deflection of the probe beam was measured with
a lock-in amplifier during cyclic voltammetry. The
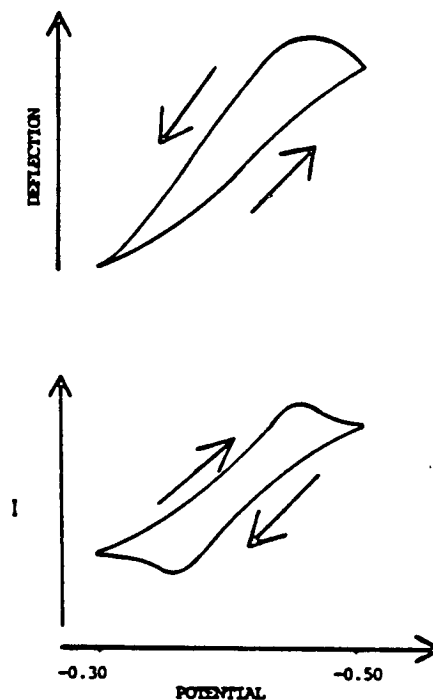results in Figure 7 show that the AC signal detects the

BQ⁻· concentration

gradient. During the

cathodic sweep, the BQ⁻·

concentration gradient

increases as the

reduction current

increases. The anodic

sweep causes the reverse

behavior as BQ⁻· is

oxidized. The spectra of

the electrolyte species

can also be measured.

Figure 8 shows the
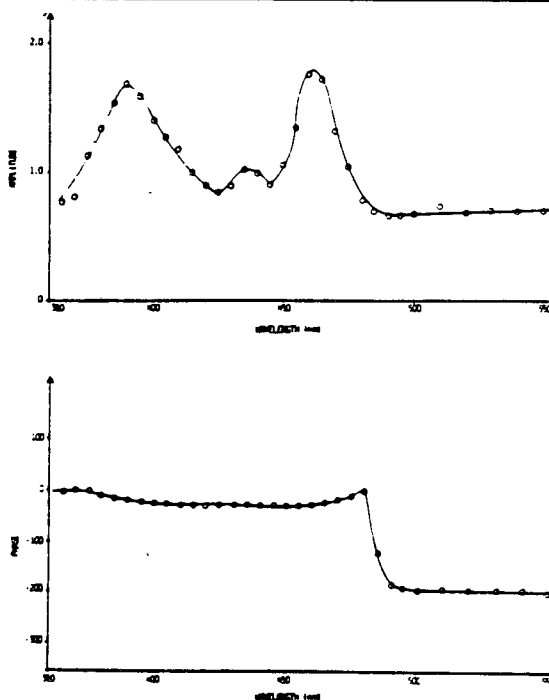
results of a spectral

Figure 8. Signal magnitude and phase as a function of wavelength. The data points were recorded during the cyclic voltammogram at -0.50 V *vs*. a Ag wire psuedo-reference electrode. [reprinted by courtesy from reference 21].

scan experiment. Each data point was recorded at -0.5 V

on the cyclic voltammogram. The absorption spectrum

shows peaks at 460 and 435 nm which correspond to the BQ⁻·

spectrum. The peak at 400 nm is attributable to BQH·,

which is produced by homogeneous chemical reaction. The

phase of the signal exhibits the 0° phase described

above. The background level is caused by the absorption

of light at the platinum electrode. The phase plot shows

that the surface signal is at ~ -200°.

For systems with electrolyte components which are

spectroscopically indistinct, an interesting possibility

is the addition of indicators to the electrolyte. For

instance, an acid-base indicator can be added to a H_2SO_4
electrolyte supported with Na_2SO_4. The indicator would
provide a distinct spectroscopic tag of the H^+
concentration gradient. The indicator would be present
at constant concentration, but its absorption coefficient
would vary with H^+ concentration. Theoretically, this is
equivalent to the cases studied above, and the
concentration gradient of H^+ could be determined. The DC
deflection would measure the bulk effect of the H_2SO_4 and
Na_2SO_4. Subtraction of the H^+ concentration gradient
from the bulk signal yields the Na^+ concentration
gradient. This method requires that the indicator does
not change the electrochemistry and is only a proposal.
We have begun to investigate this method.

E. Complications

Three minor processes can cause DC deflections,
thereby interfering with the measurement of the
concentration gradient. First, at steady state, a DC
thermal gradient which conducts heat away from the
interface is required to balance the net heat input due
to absorption of light at the electrode surface. The DC
deflection of the probe beam that this thermal gradient
causes is typically negligible. This assumption can be
verified by comparing the DC deflections while the
excitation light is off and on. Second, heat is
generated at the interface by the reversible and

irreversible heats of the electrochemical reaction, due
to the entropy change of reaction and the overpotential,
respectively (25). These effects combined are sometimes
referred to as the Peltier heat (29). Third, resistive
heating of the electrolyte can generate thermal gradients
in regions of non-uniform electrical conductivity. Few
measurements of these heat effects have been made.
Tamamushi studied the Peltier heat for the
ferri/ferrocyanide redox couple with a differential
temperature sensor (29). His results showed that for the
ferri/ferrocyanide redox couple the DC deflection of the
probe beam caused thermally by the Peltier heat was
orders of magnitude smaller than DC deflection due to the
concentration gradients (24). In most systems these
effects can probably be neglected, but their presence
should be recognized.

III. Experimental Technique

PDS has five major components: a source of excitation light, a probe beam, a position detector, an electrochemical cell, and measuring & recording equipment. (see Figure 9). When designing a PDS

Figure 9. Block diagram of PDS system showing the five major components.

system, an investigator has several options for each of these components. In the following sections, each major component will be described.

A. Sources

The source is the origin of the excitation light. The earliest PDS systems used lasers as the excitation light because their high intensity resulted in large signals. As the technique developed, broadband sources where used. Most recently, spectrally multiplexed sources have been used because of the increased sensitivity they give the PDS system.

monochromatic excitation source

The excitation sources have a variety of characteristics which make them applicable to different systems. If a tunable source is not required, a laser
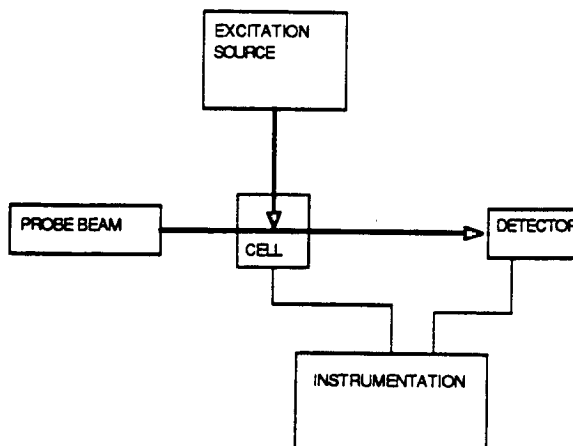
can be used as a high power monochromatic excitation
source. If only a narrow spectral region is of interest,
a dye laser can be used to provide high power excitation
light tunable over a small wavelength range. To cover a
large spectral region, a broadband light source and a
monochromator are used to produce narrow-bandwidth
excitation light. Tungsten filaments or glow bars are
used to provide approximate black-body radiation
throughout the visible and infrared. A xenon arc lamp
produces higher-intensity light than filaments, but is
limited to the visible region and exhibits intensity
fluctuations (30).

All of the monochromatic sources are modulated;
amplitude and polarization techniques have been used.
Amplitude modulation is the common technique. A
mechanical chopper produces a 50:50 on/off cycle of the
excitation light. Polarization modulation has been
reported to be a sensitive technique for measuring small
changes of surface absorption on a large background (31).
With this technique, the excitation light is applied at a
shallow angle to the electrode surface. The polarization
of the light is modulated such that the electric field
vector of the excitation light changes between being
predominantly normal to and parallel to the electrode
surface.

multiplexed excitation sources

Spectrally multiplexed sources offer higher sensitivity than monochromatic sources. The multiplexed sources mix all the wavelengths of light in the spectral region of interest into the excitation light. Because more light is applied to the sample, the signal amplitude will be higher. An appropriate deconvolution algorithm is then used to analyze the signal. Common scanning Fourier transform infrared (FTIR) spectrometers have been used in conjunction with PDS (13,32-37). The sample cell is placed in the sample compartment of the FTIR where the excitation light is focused onto the sample surface. The probe beam deflection signal is substituted for the light intensity signal normally measured by the FTIR. The FTIR deconvolutes the signal to produce an absorption versus wavelength plot.

Each wavelength is present at a different modulation frequency in the excitation light of a scanning FTIR. Since the PDS signal is dependent on modulation frequency, the absorption spectrum obtained with a scanning FTIR is distorted. To solve this problem, Smith and Palmer have developed a step-scan FTIR (33,38). This instrument mixes the excitation light such that all wavelengths are present at the same frequency, and is therefore well suited to PDS.

As the wavelength of excitation light becomes
shorter, Fourier transform interferometers become more
difficult to build. In the visible region, an
alternative is a Hadamard transform excitation source
(39). This type of transform mixes discrete wavelengths
as opposed to the continuous mixing Fourier provides.

B. Probe beam

The probe beam used is almost always a Helium Neon
laser. A small beam diameter is desirable, therefore
lasers with a $1/e^2$ diameter of less than 1 mm are
typical. Although pointing instability and intensity
fluctuations can be corrected for with methods described
below, a good probe laser should minimize these
parameters. A lens between the laser and electrode
typically focuses the beam to a diameter of 40-100 μm at
the electrode.

Most PDS systems measure the primary gradient (see
Figure 10). This gradient is formed on the side of the
electrode where the excitation light is applied. Three
alternative arrangements of the probe beam are described
below.

secondary gradient measurement

We have studied the 'secondary gradient', which is formed at the back of a thin electrode (~125 µm). Figure 10 shows the arrangement; the electrolyte is on both sides of the electrode, the excitation light is applied to the

Figure 10. Side view of primary and secondary gradients for a thermally thin electrode.

front of the electrode and the probe beam passes along the back of the electrode. Heat generated at the front surface will be conducted through the electrode into the electrolyte at the back. Because the electrode is thin (thermally), it will be at approximately uniform temperature at all times. If both sides of the electrode are at approximately the same temperature, the thermal gradient at the front, the primary gradient, and the secondary gradient will be of approximately equal magnitude and opposite sign. This result has been confirmed experimentally.
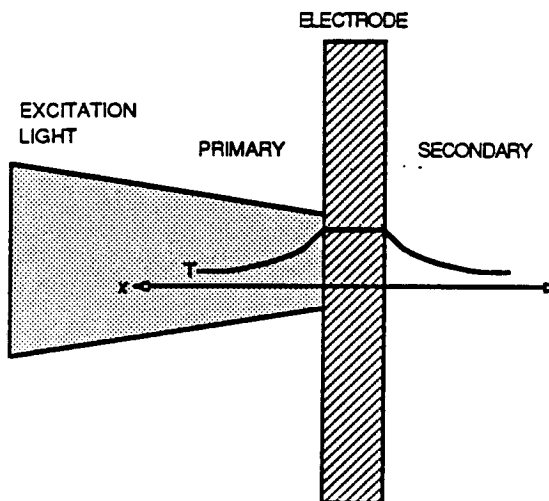
Measurements obtained with the probe beam on the back side of the electrode do not contain the component of the deflection caused by absorption of light in the electrolyte (assuming no light passes through the electrode), *i.e.* the AC deflection at 0° is eliminated.

For systems were it is not practical for the probe beam to pass along the front side of the electrode, the secondary gradient method is useful. Gas-evolving electrodes are an example. The probe beam would be chaotically deflected by bubbles at the interface. In such cases, the back side of the working electrode could ·be isolated from electrochemical reaction. For the study of thin-layer cells, it may not be practical for the probe beam to pass through the thin gap in front of the electrode. For these cases, passing the probe beam along the back of the electrode would allow the interfacial absorption to be measured.

dual beam

Several researchers (21) have used a pair of probe beams to correct for noise in the beam deflection. The major sources of noise are the pointing instability of the laser and mechanical vibrations. Figure 11 shows a dual-beam arrangement. The
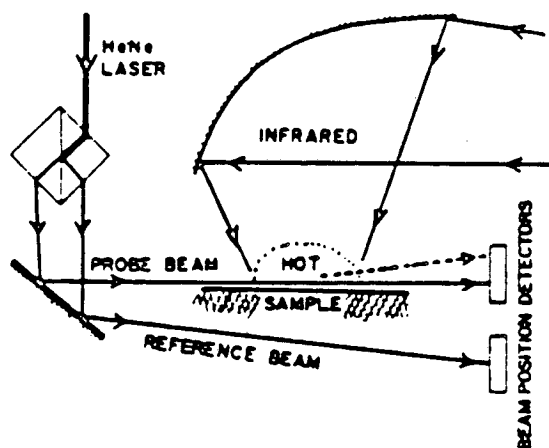

Figure 11. A dual probe beam setup. A beam splitter cube creates the two beams. The sample beam passes adjacent to the sample surface in the conventional manner. The reference beam travels a similar path. [reprinted by courtesy from reference 34]

sampling probe beam samples the electrode surface and the reference beam travels a similar path, but is isolated from the gradients that the first measures. The

deflections of the reference beam are assumed to be a
measurement of the noise. The deflections of the
reference beam are subtracted from the deflections of the
sampling beam.

   spatially multiplexed

   Fournier and Boccara have developed a spatially
multiplexed probe beam (12). The arrangement is shown in
Figure 12. The probe beam is expanded into a *ribbon*.
The ribbon samples a wide area of the electrode and
passes onto a position detector formed by a knife edge
design and a linear photodiode array (See the next
section for a description of the knife-edge position
detector). The resulting system can simultaneously
measure the beam deflection at 256 positions along the
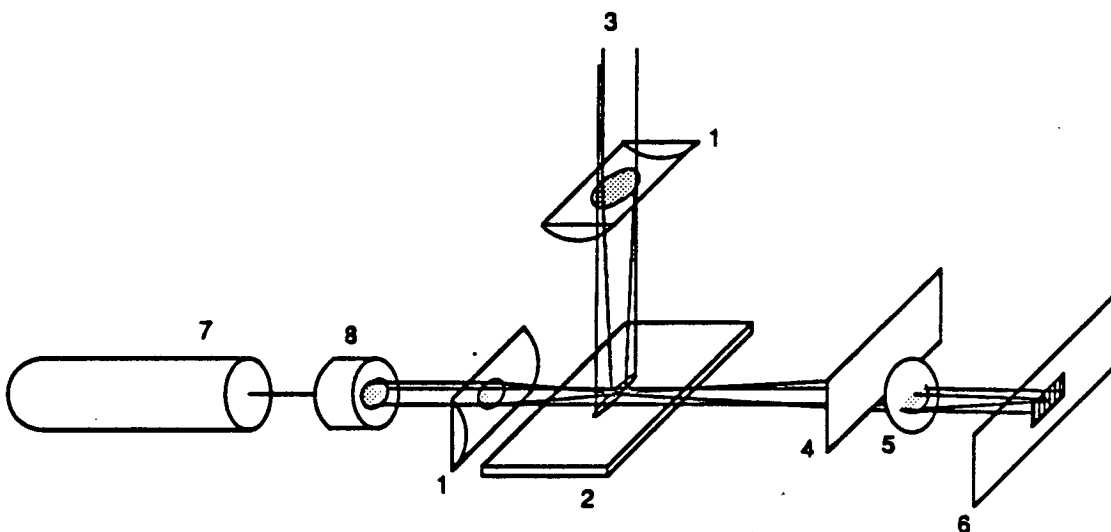width of the ribbon. This system is applicable to the

Figure 12. Schematic of spatial multiplexing. 1) cylindrical lens, 2) sample 3) excitation beam,
4) razor blade, 5) spherical lens focuses probe "ribbon" onto the detector, 6) CCD photodiode
array, 7) probe laser, 8) beam expander [adapted from reference 12]

study of electrodes with non-uniform current densities.

C. Position Detectors

The position detector is a device which produces a
voltage signal proportional to the linear displacement of
the probe beam spot along its surface. From the linear
displacement, the angular deflection can be calculated.

Typically the position detector is located within
500 mm of the electrode. Since the linear displacement
along the detector surface is equal to the angular
deflection of the probe beam multiplied by the electrode-
to-detector distance (for small angles), it may seem that
the position detector should be placed far from the cell
to produce a large linear displacement; but this is
impractical. Because the probe beam is focused to a
narrow waist at the electrode, it diverges after it
passes the electrode. The maximum distance between the
detector and electrode is therefore limited by the size
of the detector (the probe beam spot must be smaller than
the detector size). Also, increasing amounts of noise,
caused by mechanical vibrations and air currents, are
introduced as the distance between the electrode and
position detector increases.

The various position detectors used have a variety
of characteristics, making each most suitable for a given

application.   Three commonly-used position detectors are
discussed below.

knife-edge detector

The knife-edge detector is the simplest design. The
detector is made by passing the probe beam past the edge
of a razor blade onto a photodiode (hence the origin of
the name) as shown in Figure 13a. The photodiode outputs
a current proportional to the power impinging on it. As
the probe beam deflects up in the figure, more of the
probe beam passes the knife edge and the photodiode
signal increases; as the probe beam deflects down, the
photodiode signal decreases. The simplicity of this
detector is its advantage: only a photodiode and a simple
current amplifier are required. The drawbacks of this
detector are that it is linear only for small deflections
of the probe beam and is sensitive to intensity
fluctuations of the probe beam.

bicell detector

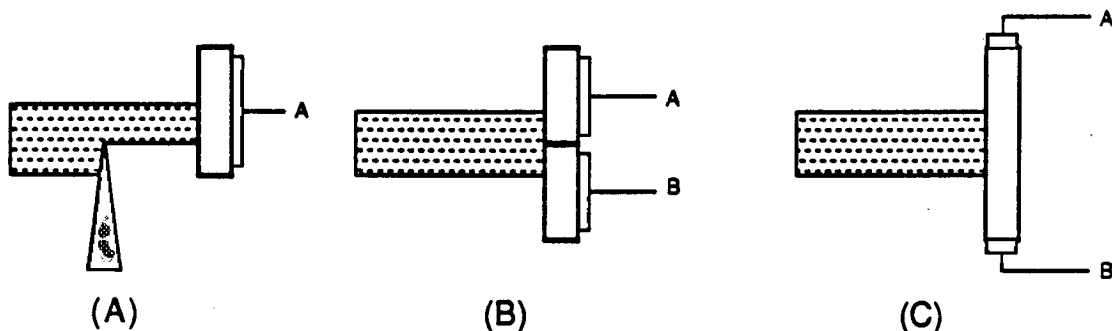The bicell position detector is shown in Figure 13b.

Figure 13. Three position detectors A) knife edge, B) bicell, and C) 1d linear.

This device consists of two photodiodes with only a thin
insulating line separating them. When the probe beam
hits the center of the detector, equal currents (i_A and
i_B) will be formed in side A and B. When the probe beam
is off-center, the currents will be unequal. A single-
axis position monitor is a commercially available device
which calculates $[i_A-i_B]/[i_A+i_B]$ (UDT model 301-DIV,
United Detector Technology, Corp.). The denominator of
this equation allows the intensity of the probe beam to
vary without causing a change in the position output.
The bicell/position monitor combination is a improvement
to the knife-edge detector. Improved linearity, and
insensitivity to intensity fluctuations of the probe beam
are provided.

1d and 2d linear position detectors

The linear position detector (LPD) is an excellent
device for PDS systems. As the name implies, this
detector has a linear response to probe beam deflections.
The 1-dimensional detector is shown in Figure 13c. The
detector is a single rectangular photodiode with
connections to the cathode at each end, and a connection
to the anode at the center. When the probe beam strikes
the photodiode currents will flow from each cathode
connection (which are equal if the spot is at the
center). A single axis position monitor is used to
calculate the $[i_A-i_B]/[i_A+i_B]$. This calculation will

determine the centroid of the beam spot along the axis of
the detector. Two-dimensional position detectors are
similar to the 1d detector, except there are four cathode
connections and one anode connection at the center of a
square photodiode. The LPD offers the advantage of
linearity. In general they are less sensitive than the
bicell.

Spear, *et. al.* report a innovative use of a single
1d linear detector in a dual probe-beam setup (40). As
described above, two probe beams can be used to correct
for noise in the probe beam deflection. Instead of using
two position detectors, the deflection of the reference
beam can be reversed with a lens. Both beams hit the
same linear position detector. The LPD detects the
intensity-weighted centroid of the light striking the
detector. The distribution of the light is unimportant.
Therefore, two probe beams symmetrically striking the
detector about the center axis will produce the same
signal as a beam striking the center of detector. If the
two beams move equally, one to the left and one to the
right, there will be no change in the signal from the
LPD. Therefore, a single detector and position monitor
can be used as a self-correcting detector for dual-probe
beam setups.

D. Electrochemical Cells

The electrochemical cell requires three windows; two windows for the probe beam, and one for the excitation light. Other than that requirement, any arrangement is possible. As one can imagine, a great variety of cell designs have been used. A few examples are described below.

normal

Two types of electrochemical cells we typically use at the Lawrence Berkeley Laboratory are shown in Figure 14: the 'single-sided' and the 'double-sided' cell. The two cells differ in the placement of the working electrode. In the single-sided cell the working electrode is mounted almost flush against the back wall of the cuvette. The probe beam passes in front of the electrode (front being the side to which the excitation light impinges). In the double-sided cell the working electrode is mounted in the center of the cell and counter electrodes are places in front and back of the working electrode. The double-sided cell allows either the primary or secondary gradient to be investigated. With respect to electrochemistry, the double-sided cell is symmetric. The same reactions occur on both sides of the electrode (in the absence of photo-effects), therefore DC deflections should be of equal magnitude and opposite sign on the two sides of the electrode.

Both cells are constructed inside 1x1x4 cm quartz flourimeter cuvettes. These cuvettes are convenient because they have five polished faces of high optical quality and are fused without the use of any adhesive, therefore, they present no contamination problems. The excitation light is focused onto the working electrode. The working electrodes are approximately 125 μm thick. The counter electrodes are platinum screens mounted on platinum wires. A gap between the screens allows the excitation light to illuminate the electrode without impediment. The reference electrode is contained in a
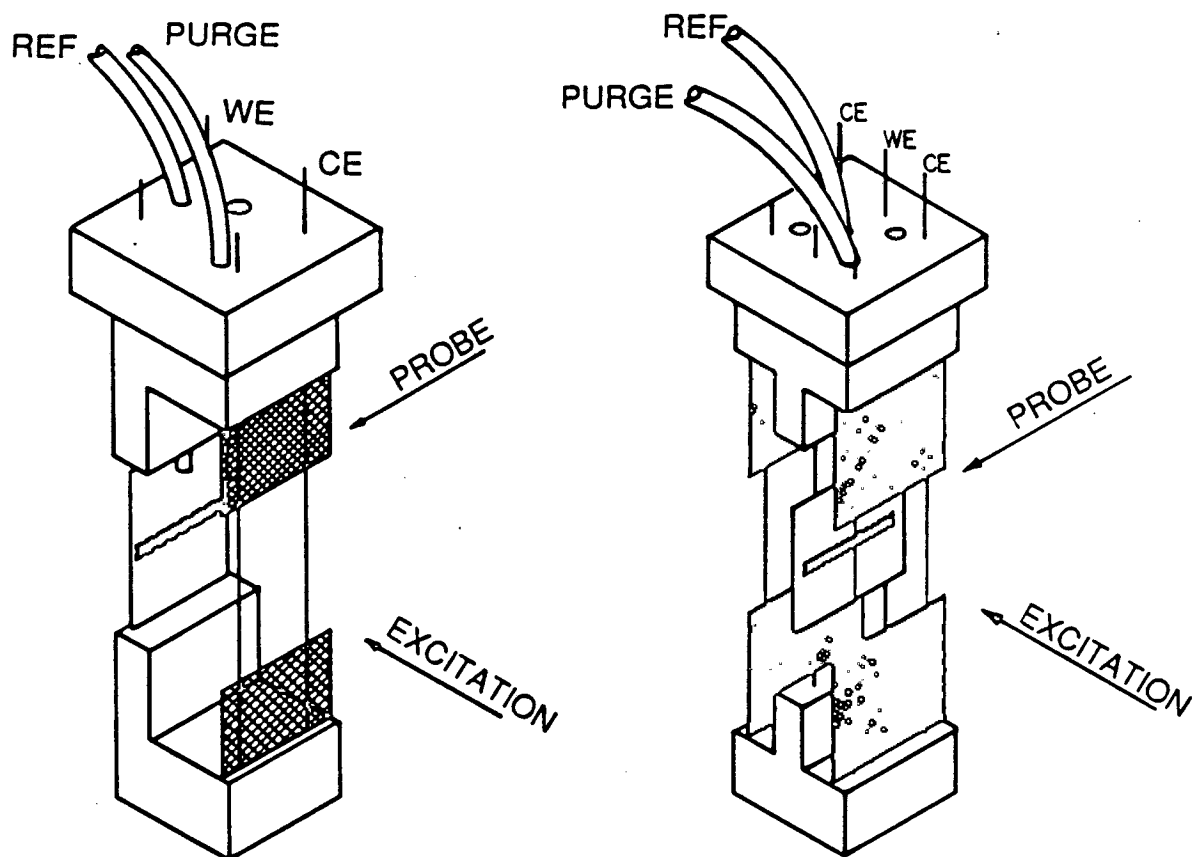

Figure 14. Diagram of a single-sided and double-sided electrochemical cells.

separate compartment filled with the same electrolyte as
that in the cuvette. A thin tube connects the cuvette to
the reference compartment. Nitrogen is bubbled through
the electrolyte as a purge gas, and during the
experiments, nitrogen is passed over the electrolyte.
The mounts which hold the electrodes and all tubes are
polytetrafluoroethylene (PTFE).

IR cells

Vibrational spectroscopy is a powerful tool for
identifying electrode surface species. Unfortunately,
most electrolytes are aqueous and water is highly
absorbing in the infrared region. This makes infrared
spectra impossible to obtain with the cells in Figure 14.
Two techniques exist for obtaining infrared absorption
spectra in aqueous environments.

One solution to the difficulty of obtaining infrared
spectra is the use of an optically transparent electrode
(OTE). A thin layer of metal, tens of Angstroms in
thickness, can be placed onto a infrared transparent
substrate. When prepared by the appropriate techniques,
the metal layer will be optically transparent. The
excitation light is then applied from the substrate side
of the electrode (see Figure 15). Smith & Palmer have
applied this technique to PDS, referred to as the reverse
mirage effect (33), to study non-electrochemical
solid/liquid interfaces. In practice OTE's are difficult

EXCITATION
LIGHT

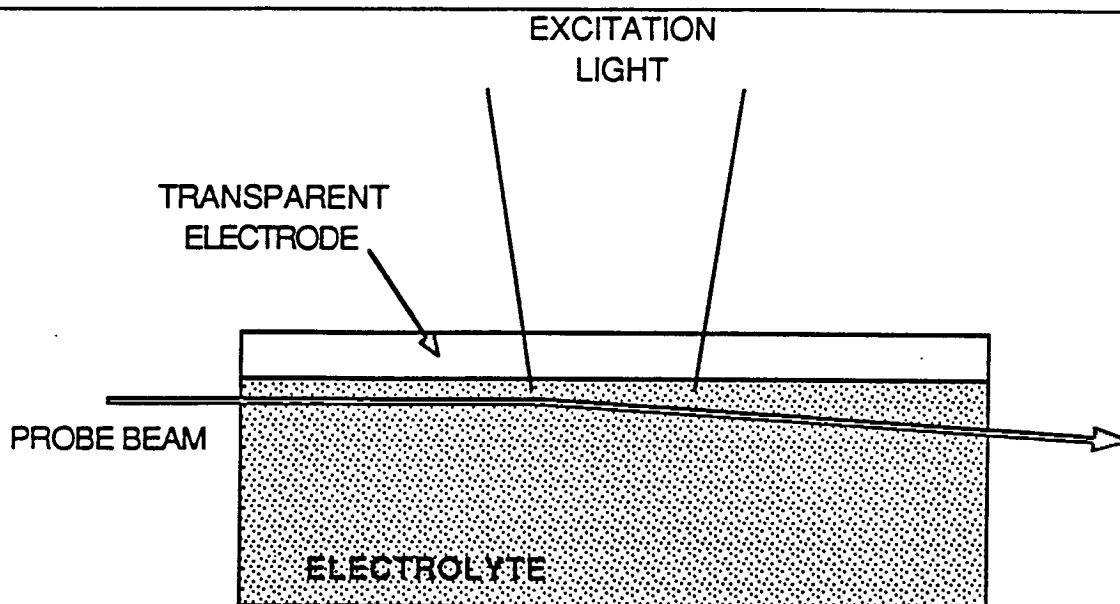TRANSPARENT
ELECTRODE

PROBE BEAM

ELECTROLYTE

Figure 15. Diagram of arrangement of probe beam, excitation light and electrode used in reverse mirage effect PDS.

to prepare, and place undesirable restrictions on electrode material.

The other solution is to use a thin-layer cell, shown in Figure 16. This technique has been used for reflection spectroscopy of polished electrodes. Nichols and Bewick (41) have developed a thin-layer flow cell which overcomes the depletion of the reactant in the electrolyte. But, for PDS it is impractical to focus a probe beam through the thin electrolyte layer required of these thin-layer cells. We developed the secondary gradient technique, described above, to solve this problem.
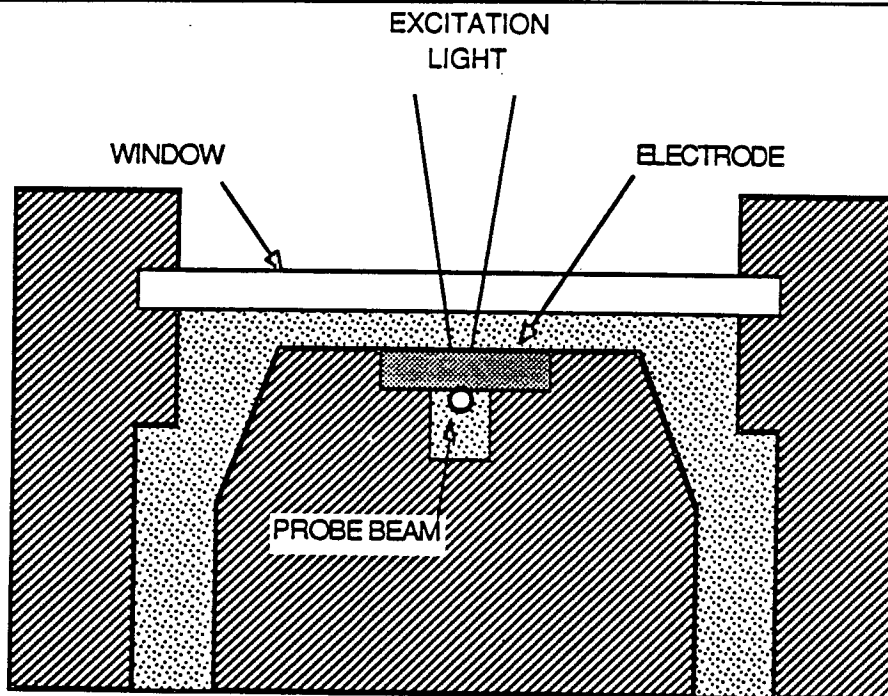
Figure 16. Cross section diagram of a thin layer cell. The probe beam travels normal to page through suitable windows in the cell body. The thickness of the electrolyte between the electrode and window is variable with 0.2 μm resolution. The gap is shown expanded for purpose of explanation, typically, the thickness is less than 5 microns.

Zinc model pore

Weaver has developed a zinc model pore cell shown in Figure 17 (42). The geometry of this cell can be conformally mapped into a cylindrical pore (43). A 2d linear position detector is used to measure the concentration gradients along both axes, simultaneously with the surface absorption. In gaps thinner than approximately 100 μm, it becomes difficult to pass a probe beam through the 1-cm-wide gap (the electrodes must be wide to minimize edge effects). For gap thicknesses less than 100 μm, the surface absorption can be measured by using the probe beam on the back of the electrode.
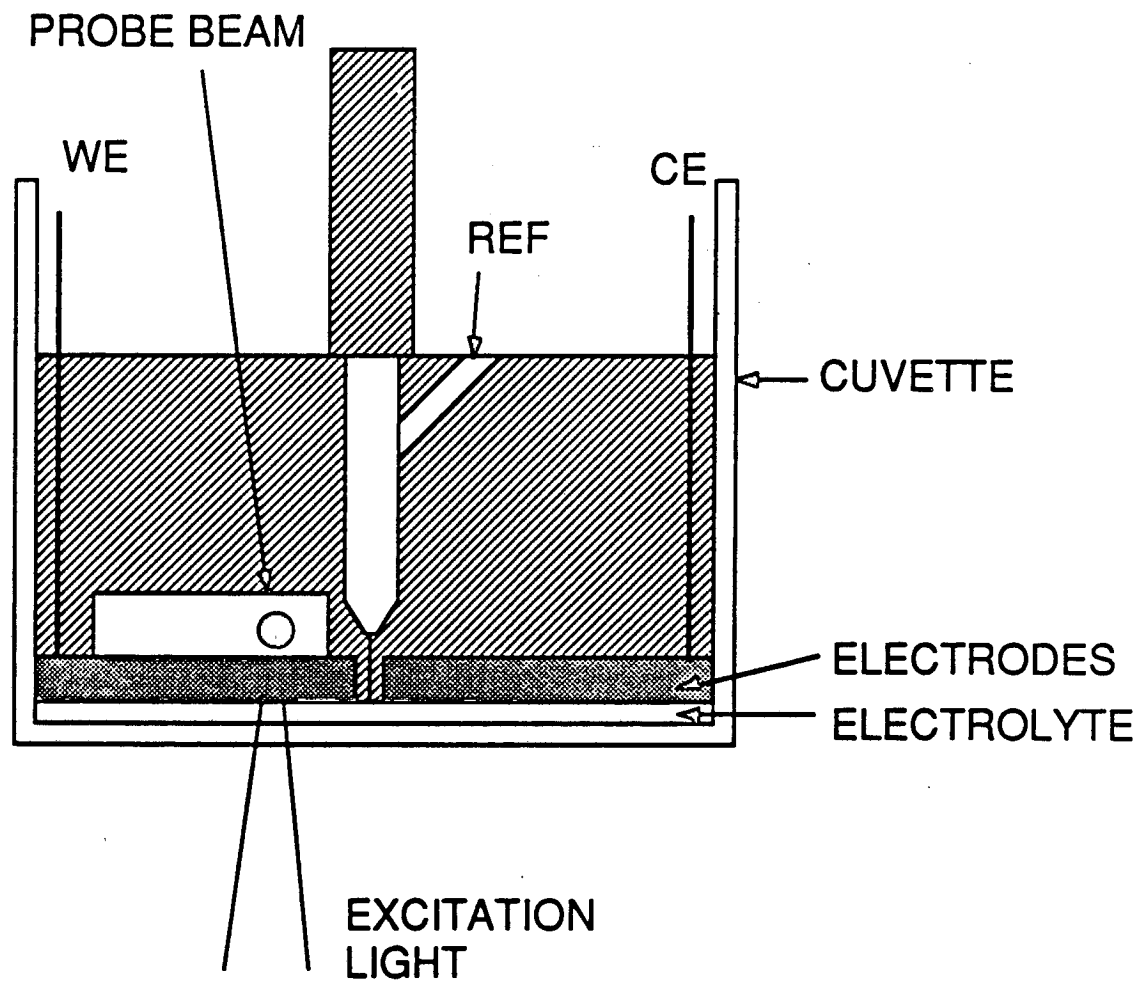
Figure 17. Cross section diagram of Zinc model pore cell. The cuvette is 2x1 cm and the two Zn electrodes are 0.9x1 cm. The gap size is controlled with a differential micrometer to be any size down to 0.5 μm with 0.2 μm resolution. The probe beam can pass through the electrolyte for gaps larger than 100 μm. For the smaller gap sizes, the probe beam passes along the back of the electrode (as shown). The reference electrode is connected thru a hole in the insulator separating the electrodes.

E. Measuring and Recording Equipment

System instrumentation varies greatly. The instrumentation used at Lawrence Berkeley Laboratory, shown in Figure 18, will be used to illustrate the basic features of a system. The experiments are controlled by, and all data are acquired by a Digital Equipment Corp. LSI-11/23 computer. A Princeton Applied Research 273 potentiostat and a Spectradata MC20 monochromator driver are controlled by the computer through an IEEE-488 interface.

The probe beam deflection signal originates at the LPD and is processed by several components. This signal contains the three components of the deflection described earlier. The first step in processing the signal is to separate the AC and DC components. Two Ithaco 1201 low-noise pre-amplifiers containing low-pass and high-pass filters accomplish this separation. The input to one pre-amplifier is AC coupled and the high-pass and low-pass filters are set to bracket the modulation frequency. Effectively all DC is removed. The remaining AC components are amplified and fed to the
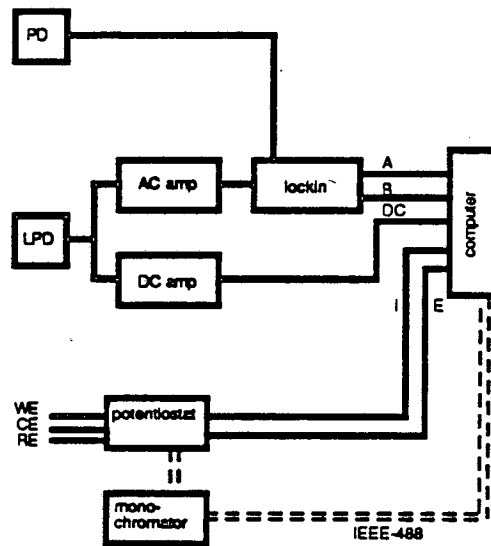
Figure 18. Block diagram of typical system instrumentation.

lock-in amplifier. The input to the second pre-amplifier is DC coupled and the low-pass filter is set at 10 Hz. Effectively all AC components are removed. This signal is amplified and fed to the computer as the DC signal.

An Ortec Ortholoc-SC 9505 two-phase lock-in amplifier is used to process the AC components of the signal. The basic function performed by the lock-in amplifier is to measure the amplitude of AC signals which are at the same frequency as a reference signal, thereby rejecting noise present at other frequencies. Another function of the lock-in amplifier is phase discrimination; the magnitude of the AC signal at a specific phase (the phase is relative to the reference signal) is measured. A two-phase lock-in amplifier measures the magnitude of the AC signal at a given phase, and the magnitude of the AC signal 90° relative to the given phase. Thereby, the lock-in amplifier can completely resolve the two AC signals at x° and 0° (described in Section II.B and II.D) when x is 90 or 270. The phase of the AC signal at x° can be adjusted to 90 or 270° by varying the chopping frequency and distance of the probe beam from the electrode (see Section II.B). After making this adjustment, the two components of the AC signal will be orthogonal, allowing the lock-in amplifier to simultaneously measure both.

experimental methods

Two types of experiments are commonly performed.
The first is the measurement of the absorption spectrum
of the interface while the electrode is held at constant
potential, and the second is the measurement of the DC
and AC signals during an electrochemical experiment while
the excitation light is held at constant wavelength.

During the first type of experiment, only the
absorption of light at the interface is measured. The
computer records the AC signal at x° at a discrete number
of wavelengths (typically every 2-5 nm) over the range of
interest. The scan is typically repeated from 4 to 15
times and the results are averaged. Because the
excitation source is not spectrally flat, *i.e.* the
intensity is not equal at all wavelengths, a correction
must be made for the spectrum of the source. Correction
is achieved using the measured spectrum from a similar
scan on an *ultra*black carbon (Spezialschwarz 4, Degussa
Corp., Teterboro, NJ). The AC signal for the electrode
is divided by the AC signal for the carbon at
corresponding wavelengths. This method of correction is
imperfect because of the slight variability of carbon
samples (44,45), but provides a close representation of
the true absorption spectrum.

The second type of experiment is an electrochemical
experiment at constant wavelength. The potentiostat is

programmed to conduct a two-part experiment. The first
part is an electrochemical pretreatment, designed
specifically for each electrochemical system to assure
that the electrode is in a reproducible state. The
second part is the electrochemical experiment, which is
the potential program of interest, *e.g.* triangular sweep,
linear sweep, *et cetera*. During the second part of the
experiment, the current, potential, DC and AC signals are
recorded. The whole experiment (pretreatment followed by
potential program) is repeated many times and the results
are averaged. Satisfactory results for experiments
involving submonolayer changes required the averaging of
40 to 50 potential sweeps.
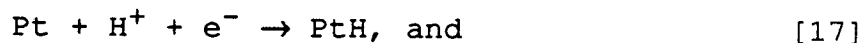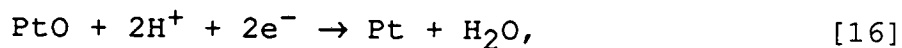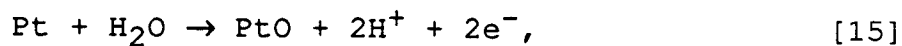
photoelectrochemical systems

PDS systems can be expanded to study
photoelectrochemical systems by adding a lock-in
amplifier to the current output of the potentiostat to
monitor the currents caused by the modulated excitation
light. These currents can be photocurrents or
photoelectrochemistry. Wagner, Wong and Mandelis have
used such a system for the study of semiconductors in
electrochemical environments (46,47).

IV. Electrochemical Systems

A. Submonolayer Studies

Electrochemical oxidation and reduction of platinum in 0.1 $\underline{M}$ perchloric acid is shown in Figure 19, and demonstrates the submonolayer sensitivity achievable with PDS (48). Before discussing the experimental results, a brief description of the electrochemistry is in order.

Moderate agreement about the electrochemistry of platinum exists in the literature (49-55). The proposed reactions are

$$Pt + H_2O \rightarrow PtO + 2H^+ + 2e^-, \qquad [15]$$
$$PtO + 2H^+ + 2e^- \rightarrow Pt + H_2O, \qquad [16]$$
$$Pt + H^+ + e^- \rightarrow PtH, \text{ and} \qquad [17]$$
$$PtH \rightarrow Pt + H^+ + e^-. \qquad [18]$$

To describe these reactions, it is convenient to start at A on the anodic sweep of the current plot, see Figure 19, where the platinum surface is pure. Formation of the oxide layer by Reaction [15] occurs during the anodic sweep from A to C. Because of the irreversibility of platinum oxidation, little happens during the cathodic sweep from C to D. Reduction of the oxide layer by Reaction [16] occurs during the cathodic sweep from D to E. From E to F a platinum hydride layer is formed by Reaction [17]. The oxidation of the hydride layer occurs during the anodic sweep from F to A.
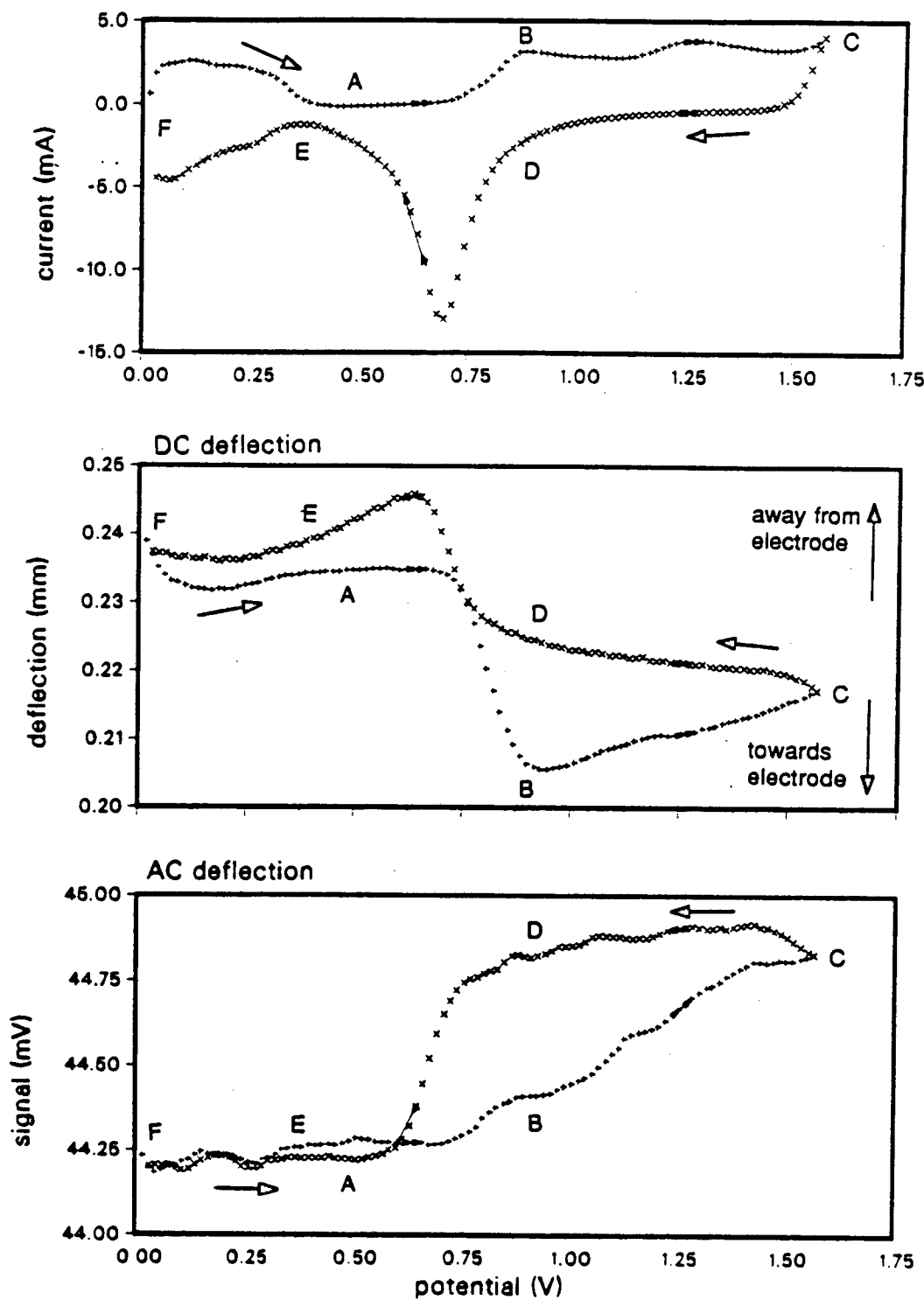
Figure 19. Triangular potential sweep from 50-1600 mV of a Pt electrode in 0.1 $\underline{M}$ $HClO_4$ at 75 $mV \cdot s^{-1}$. Pretreatment of the electrode consisted of a series of potential steps between 1600 mV and 50 mV, which insured that the electrode state is reproduced at the beginning of each sweep. The current, DC signal (concentration gradient), and AC signal (optical surface absorption) are shown. The anodic sweep data points are marked by +'s and the cathodic sweep by x's. The excitation light wavelength was 650 nm and the modulation frequency was 20 Hz. The curves are the average of 40 sweeps.

The DC deflection results give some interesting insight into the electrochemistry. To interpret this curve one must keep in mind that the refractive index of perchloric acid increases as the acid concentration increases and that the probe beam is deflected towards the region of higher refractive index. Again, starting from A, a deflection towards the electrode is seen from A to B. This is consistent with Reaction [15] which consumes water and releases protons, resulting in an increased acid concentration near the electrode. Ignore for a moment the change from B to C; this is discussed subsequently. From C to D a slow relaxation of the gradient by diffusion is seen. From D to E, Reaction [16] reverses the direction of the gradient. Reactions [17] and [18] cause slight effects. The magnitude of the gradients for these reactions is smaller because of the unusually fast mechanism of proton transport (56) and because no water is involved in the reactions.

During the anodic sweep from B to C, it is seen that the deflection of the probe beam towards the electrode is decreasing. This behavior contradicts what would be expected from Reaction [15]. The explanation is found in a two-step oxidation process, often suggested in the literature (54,57), where the first step is the formation of a hydroxide

$$Pt + 2H_2O \rightarrow Pt(OH)_2 + 2H^+ + 2e^- \qquad [19]$$
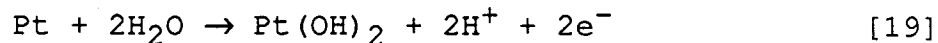
followed by the dehyration to the oxide

$$Pt(OH)_2 \rightarrow PtO + H_2O. \qquad [20]$$
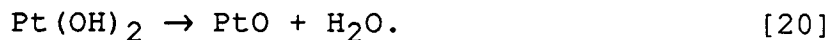
The data in Figure 19 support this mechanism. From A to B during the anodic sweep, a fraction of the platinum surface is oxidized according to Reaction [19], causing the acid concentration near the electrode to increase. From B to C the release of H_2O by Reaction [20] causes the electrolyte near the electrode to be diluted. Also from B to C, the remaining unoxidized fraction of the platinum surface is oxidized by Reaction [15].

Of interest is the location of the zero DC deflection on Figure 19. Theoretically, by measuring the position of the probe beam when the cell is at open circuit, the rest position of the probe beam would be determined. This method has been tried, but yields random results. Either charging of the double layer, or movement of the electrode when the electrical circuit is made, could be the source of the random behavior. Despite this problem, it is probable that the flat region near A where no electrochemical reaction occurs, is the rest position of the probe beam.

The AC deflection detects the formation of the oxide film. The absorption at the surface increases as the oxide film is formed from A to C. The oxide film remains

fairly stable during the cathodic sweep from C to D. The
absorption then quickly decreases as the oxide film is
reduced, from D to E. The value of the AC signal at E is
the same value as at A. The presence of the hydride film
causes no change in the absorption. These results are in
good agreement with similar photoacoustic spectroscopy
(PAS) experiments (50). It should be noted that the
absorption signal contains a large background (the origin
of the AC graph is not 0) and is only changing
approximately 2% during this experiment. A measurement
of the charge consumed during oxidation of the surface
confirmed that the signal change from A to C is caused by
the formation of a single molecular layer (monolayer) of
PtO (it is possible for more than a monolayer to form).
The AC signal in Figure 19 is a root-mean-square voltage,
as measured by the lock-in amplifier. An AC signal of
44.25 mV (at A) corresponds to a peak-to-peak deflection
of 3.7 μm. These AC deflections are an order of magnitude
smaller than the DC deflections.

The possible effect of the reversible and
irreversible heat of reaction and ohmic heating of the
electrolyte has been considered. Partial molar entropies
of the electrochemical species are required to calculate
the heat generated at an interface. It is questionable
if the partial molar entropy of ionic species can be
determined (25); therefore, approximate calculation of

the reversible heat of reaction for oxidation of Pt to
PtO was made assuming that the heat effects at the
counter electrode (hydrogen evolution) were negligible.
Under this approximation, the entropy change for the
entire cell is assigned to the working electrode. Using
literature values (58), the entropy change for platinum
oxidation is 18.0 cal mol^{-1} K^{-1}. The oxidation current
is approximately 0.25 mA (see Figure 19), the temperature
is 290 K, and the macroscopic area of the electrode is
1.4 cm^2. From these values, the reversible heat of
reaction is approximated to be 0.02 mW·cm^{-2}. The
irreversible heat of reaction is the product of the
overpotential and current (25). Assuming the
overpotential for the platinum oxidation reaction is 300
mV, the irreversible heat of reaction is 0.05 mW·cm^{-2}.
The measured resistance of the cell is approximately 10
Ω. This resistance would result in 0.4 μW being
dissipated in the electrolyte by ohmic heating per square
centimeter of electrode. These three power intensities
are more than four orders of magnitude smaller than the
intensity of the excitation light. This leads to the
tentative conclusion that for platinum oxidation the
reversible and irreversible heats of reaction and the
ohmic heating do not complicate the analysis of the PDS
signals.

B. Metal Oxidation/Reduction Studies

Cyclic voltammetry and PDS of copper in alkaline electrolyte is shown in Figure 20 (59,60). This experiment demonstrates the four signals which can be simultaneously measured with PDS: the figure shows, from top to bottom, the current response, the concentration gradient measured by the DC deflection signal, the absorption of light in the electrolyte measured by the AC at 0° signal, and the absorption of light at the interface measured by the AC at x° signal.

The peaks on the anodic sweep of the current curve marked AI and AII represent the oxidation of copper to insoluble copper oxides or hydroxides (61-65). Although the products generated at AI and AII are disputed, it is agreed that the reactions consume hydroxide ions from the electrolyte (60) and result in a lower refractive index near the electrode. During both AI and AII, the DC curve shows that the beam is deflected away from the electrode. The positive deflection at AII is preceded by a negative deflection which will be discussed below. The peaks on the cathodic sweep of the current curve marked CI and CII are the reduction of the oxides or hydroxides, formed at AI and AII, back to pure copper. These reactions are the reverse of the oxidation and cause the DC deflection to be in the opposite direction.

An interesting feature is marked X on the DC curve. This deflection towards the electrode indicates that the refractive index adjacent to the electrode has increased relative to that of the bulk electrolyte. Dissolution of a soluble species (probably bicuprate ion) from the surface explains this behavior (60). This demonstrates the ability of PDS to detect processes not discernable from the current response.
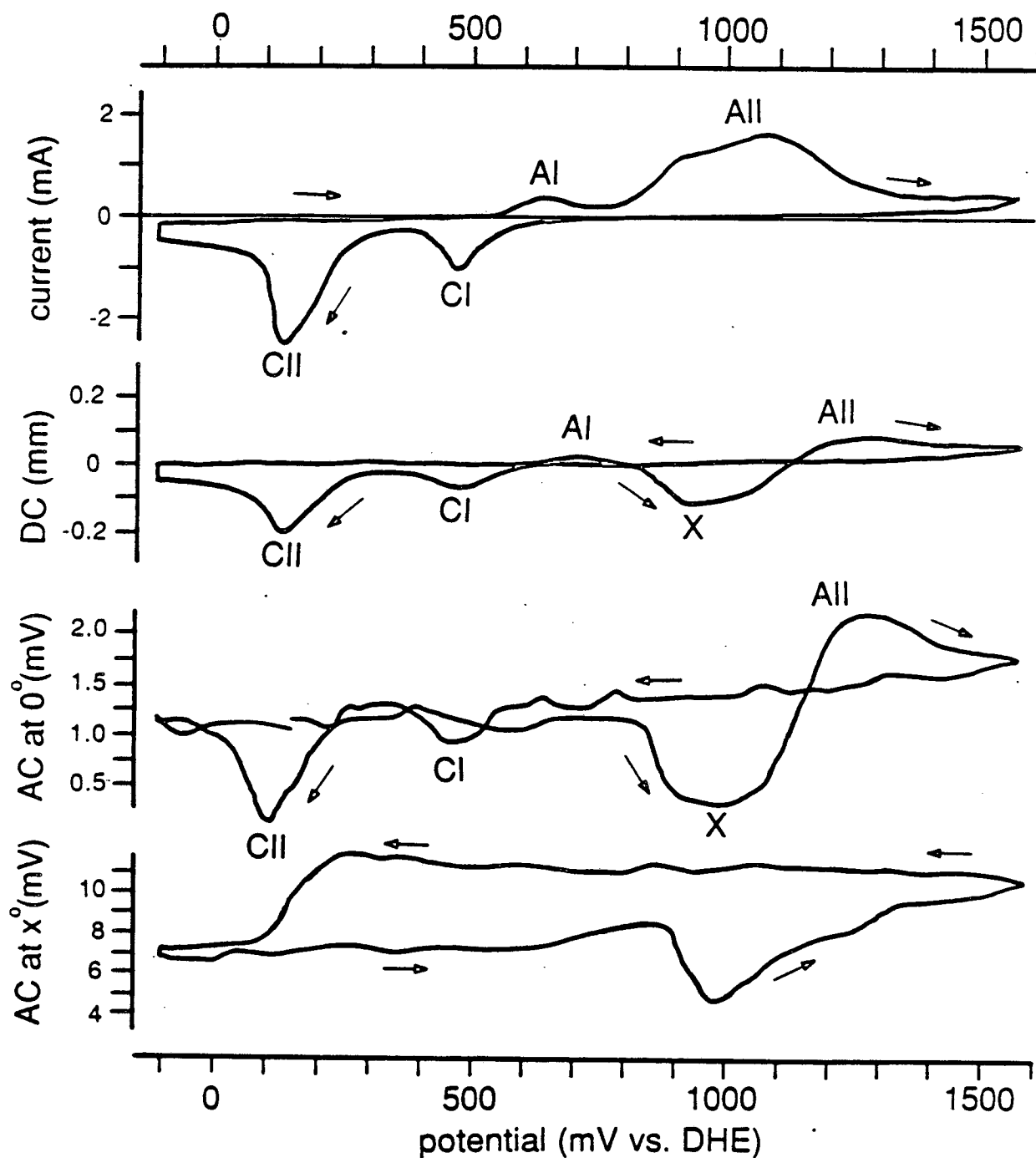
Figure 20. Cyclic voltammetry of a Cu electrode in 0.1 $\underline{M}$ KOH from -100 to 1600 mV at 20 mV·s^{-1}. Potentials refer to a DHE in the same electrolyte. The convention for the DC deflection is the same as in Figure 19, up is away from the electrode and down is towards the electrode. The excitation wavelength was 550 nm and the modulation frequency was 20 Hz. The curves are single traces recorded directly on a chart recorder.

It is proposed that the AC signal at 0° is being caused by absorption of light by the species in the concentration gradient. The AC signal at 0° follows the behavior of the DC deflection, *i.e.* when a concentration gradient is detected by the DC deflection, the AC signal at 0° also indicates the presence of a concentration gradient. A consistent explanation is that the absorption of the excitation light by potassium hydroxide is causing the signals at AI, AII, CI, and CII; and that absorption by the unknown soluble species is causing the signal at X. This experiment could be repeated at a series of wavelengths to determine the absorption spectrum of the species which are causing the concentration gradient. The AC signal at 0° shows a background signal caused by either the focusing of the excitation light, a steady background concentration gradient, or incomplete resolution of the two AC components. Further experiments are required to identify the source of this background signal.

The AC signal at x° was recorded simultaneously and shows that the two AC signals are effectively separated from each other. Briefly, the AC signal at x° indicates the formation of the oxide layer at AII. The oxide layer is present until it is reduced at CII. Further discussion of the AC signal at x° can be found in Reference 60.

C. Photocorrosion of Semiconductors

Royce, *et. al.* studied the photocorrosion of CdTe single crystals (24) in acidified $SnCl_2$ electrolyte at open circuit. Figure 21B shows the normalized near-IR spectra of the CdTe crystal before and after treatment. The spectrum of the untreated crystal is characteristic of a crystal with the correct stoichiometry. The photocorrosion reaction oxidizes Cd which dissolves into the electrolyte and results in a Te-excess in the crystal. The spectrum of the treated crystal is characteristic of Te-excess.

The above results were compared with PDS spectra of CdTe films prepared on insulating and conducting substrates, shown in Figure 21A. The comparison shows that the films prepared on insulating substrates have a spectrum corresponding to that of the single crystal with correct stoichiometry, and the films prepared on
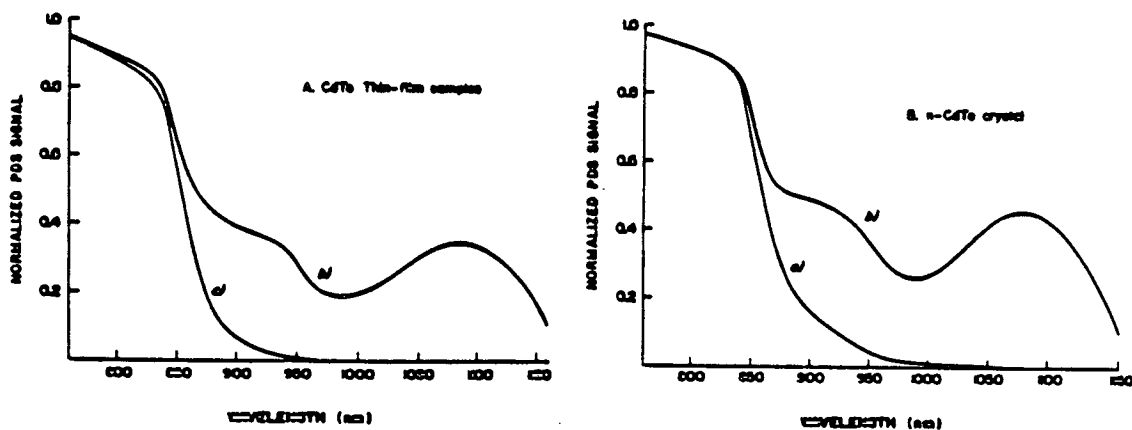

Figure 21 (A) CdTe thin film spectra a) insulating substrate, b) conducting substrate. (B) CdTe single crystal spectra a) before treatment b) after illumination with defocused HeNe laser light for 20 min. [reprinted by courtesy from reference 24]

conducting substrates have a spectrum corresponding to

that of the single crystal with the Te-excess.

V. Conclusions

The results discussed above demonstrate the versatility of the PDS technique for *in situ* and non-intrusive spectro-electrochemical measurements. The technique uses low-intensity illumination, which is safe for use with any photo-inactive electrode, to measure the surface absorption spectrum. Changes in the interfacial absorption coefficient and concentration gradients attributable to the reaction of sub-monolayer quantities have been measured.

PDS excels where reflection spectroscopies fail: As the reflectivity of the electrode decreases, *e.g.* dispersed platinum, or carbon, the reflection signal decreases whereas the PDS signal increases. The ability to separate the electrolyte absorption from the surface absorption based on the phase difference is a major advantage compared to reflection-based spectroscopies.

PDS is a promising technique for obtaining *in situ* vibrational spectra of electrode surfaces. Raman spectroscopy is an alternative method of obtaining vibrational spectra, but because the Raman scattering selection rules are different than the absorption selection rules, an absorption technique is needed. Also, the surface enhancement required for monolayer studies by Raman methods is only applicable to certain metals.

PDS is a relatively new spectroscopy and its application to electrochemical systems is even more recent. This chapter illustrates the wealth of information about electrochemical systems the technique provides. A goal for the future is increased sensitivity. This would allow faster electrochemical processes to be studied.

Acknowledgements

References

1. A.C. Boccara, D. Fournier, and J. Badoz, Topical Meeting on Photoacoustic Spectroscopy, Ames, IA, Aug. 1979, Optical Society of America, 1979. {kk low first pds}

2. A.C. Boccara, D. Fournier, and J. Badoz, *Appl. Phys. Lett.*, **36**, 130 (1980).

3. N.M. Amer, *J. De Physique*, **44**, C6-185 (1983).

4. D. Fournier, A.C. Boccara, N.M. Amer, and R. Gerlach, *Appl. Phys. Lett.*, **37**, 591 (1980).

5. J.A. Sell, *Photothermal Investigations of Solids and Fluids*, Academic Press, Berkeley, 1989.

6. A.C. Boccara, D. Fournier, W. Jackson, and N.M. Amer, *Opts. Lett.*, **5**, 377 (1980).

7. H.L. Fang and R.L. Swofford, "The Thermal Lens in Absorption Spectroscopy", *Ultrasensisitve Laser Spectroscopy*, D.S. Kliger (ed.), Academic Press, San Francisco, 1983.

8. "In Situ Characterization of Electrochemical Processes", Publication NMAB 438-3, National Materials Advisory Board, Commission on Engineering and Technical Systems National Research Council, National Academy Press, Washington, D.C., 1987.

9. M.J. Armstrong and R.H. Muller, *J. Electochem. Soc.*,
   136, 584 (1989).

10. M. Born and E. Wolf, *Principles of Optics*, Pergamon
    Press, Oxford (1970).

11. W.B. Jackson, N.M. Amer, A.C. Boccara, and D.
    Fournier, *Appl. Opt.*, **20**, 1333 (1981).

12. D. Fournier and A.C. Boccara, "Basic Physical
    Principles", *Photothermal Investigations of Solids
    and Fluids*, J.A. Sell (ed.), Academic Press,
    Berkeley, 1989.

13. D. Fournier, A.C. Boccara and J. Badoz, *Appl. Optics*,
    21, 74 (1982).

14. A. Mandelis and B.S.H. Royce, *Appl. Optics*, **23**, 2892
    (1984).

15. J.C. Murphy and L.C. Aamodt, *J. Appl. Phys.*, **51**, 4580
    (1980).

16. S. Mandelis, *J. Appl. Phys.*, **54**, 3404 (1983).

17. L.C. Aamodt and J.C. Murphy, *J. Appl. Phys.*, **54**, 581
    (1983).

18. R. Gupta, "The Theory of Photothermal Effects in
    Fluids", *Photothermal Investigations of Solids and*

Fluids, J.A. Sell (ed.), Academic Press, Berkeley, 1989.

19. A. Rosencwaig and A. Gersho, *J. Appl. Phys.*, **47**, 64 (1976).

20. N.C. Fernelius, *J. Appl. Phys.*, **51**, 650 (1980).

21. J. Pawliszyn, M.F. Weber, M.J. Dignam, A. Mandelis, R.D. Venter, and S. Park, *Anal. Chem.*, **58**, 239 (1986).

22. E.L. Lasalle, F. Lepoutre and J.P. Roger, *J. Appl. Phys.*, **64**, 1 (1988).

23. J. Pawliszyn, *Anal. Chem.*, **60**, 1751 (1988).

24. B.S.H. Royce, D. Voss, and A.Bocarsley, *J. de Physique*, **44**, C6-325 (1983).

25. J. Newman, *Electrochemical Systems*, Prentice-Hall, Englewood Cliffs, 1973.

26. D.H. Angell and T. Dickinson, *J. Electroanal. Chem.*, **35**, 55 (1972).

27. F. Decker, R.T. Neuenschwander, C. Cesar, and A.F.S. Penna, *J. Electroanal. Chem.*, **228**, 481 (1987).

28. J. Pawliszyn, M.F. Weber, M.J. Dignam, A. Mandelis, R.D. Venter, and S. Park, *Anal. Chem.*, **58**, 236 (1986).

29. R. Tamamushi, *J. Electroanl. Chem.*, **65**, 263 (1975).

29. A. Bard and L. Faulkner, *Electochemical Methods*, Wiley, New York, 1980.

30. R.L. Cochran and G.M. Hieftje, *Anal. Chem.*, **49**, 2040 (1977).

31. J.P. Roger, D. Fournier and A.C. Boccara, *J. De Phys.*, **44**, C6-313 (1983).

32. M. Peoples, M. Smith, and R. Palmer, *Appl. Spec.*, **41**, 1257 (1987).

33. M.J. Smith and R.A. Palmer, *Appl. Spec.*, **41**, 1106 (1987).

34. M.J.D. Low and M. Lacroix, *Infrared Phys.*, **22**, 139 (1982).

35. M.J.D. Low, M. Lacroix and C. Morterra, *Appl. Spec.*, **36**, 582 (1982).

36. P.G. Varlashkin, M.J.D. Low, G.A. Parodi and C. Morterra, *Appl. Spec.*, **40**, 636 (1986).

37. M.J.D. Low and C. Morterra, *Appl. Spectrosc.*, **41**, 280 (1987).

38. C.J. Manning, M.J. Smith, R.A. Palmer and J.L. Chao, "Phase Analysis of Photothermal Spectra Using Step-scan FTIR", Paper H97 presented at the 15th Annual

Meeting of the Federation of Analytical Chemistry
and Spectroscopy Societies, Boston, 1988.{244}

39. M. Harwit and N.J.A. Sloane, *Hadamard Transform Optics*, Academic Press, New York, 1979.

40. J. Spear, R.E Russo and R.J. Silva, *App. Spec.*, **42**, 1103 (1988).

41. R.J. Nichols and A. Bewick, "SNIFTIRS with a Flow Cell - A Clear Identification of the Intermediates in Methanol Oxidation on Pt", Paper presented at the 39th Annual Meeting of the International Society of Electrochemistry, Glasgow, 1988.

42. J. Weaver, unpublished results.

43. T. Katan, J.R. Savory and J. Perkins, *J. Electrochem. Soc.*, **126**, 1835 (1979).

44. S.M. Riseman and E.M. Eyring, *Spec. Lett.*, **14**, 163 (1981).

45. M.J.D. Low and G.A. Parodi, *Spec. Lett.*, **13**, 663 (1980).

46. R.E. Wagner, V.K.T. Wong, and A. Mandelis, *Analyst*, **111**, 299 (1987).

47. A. Mandelis, "Electrochemical Systems", *Photothermal Investigations of Solids and Fluids*, J.A. Sell (ed.), Academic Press, Berkeley, 1989.

48. R.E. Russo, J.D. Rudnicki, F.R. McLarnon and E.J. Cairns, "In Situ Characterization of Electrochemical Processes Using Optical Probe Beam Deflection Spectroscopy", Paper E31 presented at the 15th Annual Meeting of the Federation of Analytical Chemistry and Spectroscopy Societies, Boston, 1988.

49. K.A. Striebel, F.R. McLarnon and E.J. Cairns, "Oxygen Reduction in Fuel Cell Electrolytes", Lawrence Berkeley Laboratory Report 24340, December 1987.

50. J.K. Dohrmann and U. Sander, *J. De Physique*, **44**, C6-281 (1983).

51. Y.B., Vassiliev, V.S. Bagotzky and V.A. Gromyko, *J. Electroanal. Chem.*, **178**, 247 (1984).

52. V.S. Bagotski and M. Tarasevich, *J. Electroanal. Chem.*, **101**, 1 (1979).

53. H. Angerstein-Kozlowska, B.E. Conway and W.B.A. Sharp, *J. Electroanal. Chem.*, **43**, 9 (1973).

54. S. Gilman, "The Anodic Film on Platinum Electrodes", *Electroanalytical Chemistry, v.2*, A.J. Bard (ed.), .Marcel Dekker, New York, 1967.

55. R. Woods, "Chemisorption at Electrodes: Hydrogen and Oxygen on Noble Metals and Their Alloys", *Electroanalytical Chemistry, v.9*, A.J. Bard (ed.), Marcel Dekker, New York, 1967.

56. J.O'M. Bockris and A.K.N. Reddy, *Modern Electrochemistry, vol. 1*, Plenum, New York, 1977.

57. L.D. Burke and V.J. Cunnane, *J. Electrochem. Soc.*, **133**, 1657 (1986).

58. R.C. Weast, ed., *CRC Handbook of Chemistry and Physics, 68th ed.*, CRC Press, Boca Raton, 1987.

59. R.E. Russo, F.R. McLarnon, J.D. Spear, and E.J. Cairns, "Observation of Concentration and Thermal Gradients at the Electrode/Electrolyte Interface Using Photothermal Deflection Spectroscopy", Paper 731 presented at the 170th Meeting of the Electrochemical Society, San Diego, 1986.

60. R.E. Russo, F.R. McLarnon, J.D. Spear, and E.J. Cairns, *J. Electrochem. Soc.*, **134**, 2783 (1987).

61. J.C. Hamilton, J.C. Farmer and R.J. Anderson, *J. Electrochem. Soc.*, **133**, 739 (1986).

62. H.-H. Strehblow and B. Titze, *Electrochim. Acta*, **25,** 839 (1980).

63. U. Sander, H.-H. Strehblow and J.K. Dohrmann, *J. Phys. Chem.*, **85,** 447 (1981).

64. C.-H. Pyun and S.-M. Park, *J. Electrochem. Soc.*, **133,** 2024 (1986).

65. J.C. Hamilton, J.C. Farmer and R.J. Anderson, *J. Electrochem. Soc.*, **133,** 739 (1986).

Index